



## Modelling braided river morphodynamics using a particle travel length framework

Alan Kasprak<sup>1,2</sup>, James Brasington<sup>3</sup>, Konrad Hafen<sup>2,4</sup>, Richard D. Williams<sup>5</sup>, and Joseph M. Wheaton<sup>2</sup>

5 <sup>1</sup>US Geological Survey, Southwest Biological Science Center, Grand Canyon Monitoring and Research Center, Flagstaff, Arizona, 86001, USA

<sup>2</sup>Department of Watershed Sciences, Utah State University, Logan, Utah, 84322, USA

<sup>3</sup>Te Waiora, Institute for Freshwater Management, University of Waikato, Hamilton 3240, New Zealand

<sup>4</sup>Water Resources Program, University of Idaho, Moscow, Idaho, 83844, USA

10 <sup>5</sup>School of Geographical and Earth Sciences, University of Glasgow, Glasgow, G12 8QQ, UK

*Correspondence to:* Alan Kasprak ([akasprak@usgs.gov](mailto:akasprak@usgs.gov))

**Abstract.** Numerical models that predict channel evolution are an essential tool for investigating processes that occur over timescales which render field observation intractable. The current generation of morphodynamic models, however, either oversimplify the relevant physical processes, or in the case of more physically-complete CFD based codes, have computational overheads that restrict severely the space-time scope of their application. Here we present a new, open-source, hybrid approach that seeks to reconcile these modelling philosophies. This framework combines steady-state, two-dimensional CFD hydraulics with a rule-based sediment transport algorithm to predict particle mobility and transport paths which are used to route sediment and evolve the bed topography. Data from two contrasting natural braided rivers (Rees, New Zealand and Feshie, United Kingdom) were used for multi-scalar model verification incorporating reach-scale quantitative morphological change budgets and volumetric assessment of different braiding mechanisms. The model was able to simulate eight of ten empirically observed braiding mechanisms from the parameterized bed erosion, transport, and deposition. Representation of bank erosion and bar edge trimming necessitated the inclusion of a lateral channel migration algorithm. Comparisons between simulations based on steady effective discharge versus event hydrographs represented as a series of steady states were found to only marginally increase the predicted volumetric change, with greater deposition offsetting erosion. A decadal-scale simulation indicates that accurate prediction of event-scale scour depth and subsequent deposition present a methodological challenge because the predicted pattern of deposition may never 'catch up' to erosion if a simple path-length distribution is employed, thus resulting in channel over-scouring. It may thus be necessary to augment path length distributions to preferentially deposit material in certain geomorphic units. We anticipate that the model presented here will be used as a modular framework to explore the

15  
20  
25  
30



effect of different process representations, and as a learning tool designed to reveal the relative importance of geomorphic transport processes in rivers at multiple timescales.

## 1 Introduction

5 The dearth of morphodynamic models that resolve the bar-scale morphology of braided, gravel-bed rivers remains a first-order weakness in fluvial geomorphology. Indeed, since prediction is generally perceived to be the pinnacle of scientific enquiry, the limitations associated with existing modelling frameworks that can be used to inform management and natural hazard assessment of braided rivers restrict the contribution that our science can make to addressing societal needs (Wilcock and Iverson, 2003). Focusing model development on braided rivers is  
10 paramount since, in principle, if a numerical framework can predict the evolution of multiple channels and bars during high-flow events in these multi-thread rivers then the same framework should be transferable to single-thread rivers. Major progress has been made in applying contemporary measurement technologies to quantify the morphodynamics of braided rivers at the timescale of individual to sequences of high-flow events ( $10^{-2}$ - $10^0$  years; Lane et al., 2003; Wheaton et al., 2013; Williams et al., 2011; Lallias-Tacon et al., 2014; Williams et al., 2015).  
15 Prediction is, however, needed at the mesoscale (broadly  $10^0$ - $10^2$  km and  $10^1$ - $10^3$  years; Brasington and Richards, 2007), which exceeds the scale of feasible field-based monitoring campaigns. There have been considerable advances in modelling realistic bar-scale morphology of fine-grained braided rivers at the mesoscale (Nicholas, 2013a; Schuurman et al., 2013; Schuurman et al., 2015) but models that resolve bar-scale morphology of gravel-bed rivers at timescales greater than single high-flow events (Williams et al., 2016b) remains challenging.  
20 Furthermore, while ‘physics-based’ (Nicholas, 2013b) approaches to simulation have been successful for fine-grained rivers, such approaches have high computational overheads necessitating the use of high performance computing resources and restricting their use for exploratory applications (e.g. Nicholas et al., 2013a). The additional computational demand of simulating sediment mixtures, combined with the extant problems of spatial parameterization of sediment character, limit the scope of comparable ‘physics-based’ approaches to gravel-bed  
25 river simulations. There is therefore a need to develop an alternative, computationally efficient morphological modelling framework, capable of reproducing realistic bar-scale morphodynamics of gravel-bed braided rivers over geomorphologically meaningful timescales ( $10^1$ - $10^3$  years).

A variety of spatially-distributed morphodynamic modelling frameworks have been developed to address this  
30 problem and are reviewed in depth by Williams et al. (2016a). Current approaches have been broadly assigned into one of two philosophical categories. The first involves simplifying and abstracting physical processes using a



set of rules or simplified algorithms, giving rise to so-called ‘reduced complexity’ models, often in the form of cellular automata models (RC/CA; Murray and Paola, 1994; Coulthard et al., 2002; Thomas and Nicholas, 2002). These rule-based models offer high computational efficiency, allowing calculations over wide spatial and long temporal scales (e.g., Nicholas and Quine, 2007; Thomas et al., 2007; Ziliani et al., 2013), but at the expense of physical explanation and morphological fidelity. The alternative second subset of models are widely referred to as ‘physics-based’, and are driven by computational fluid dynamics schemes (CFD; Bates et al., 2005) typically involving two-dimensional approximations of solutions to the Navier-Stokes equations. Bed shear stress is used as a measure of the friction force imposed by flow to scale bedload transport. The direction and distance of bedload transport is calculated based upon the flow field and parameterizations are employed to represent gravity driven sediment transport, particle settling and remobilization effects. The Exner equation (Paola and Voller, 2005) is then used to calculate bed elevation change from local sediment flux divergence. This ‘physics-based’ approach to calculating morphodynamic evolution comes at the cost of significantly increased computational overheads, particularly for graded sediment. Nonetheless, physics-based models have been widely applied to simulate fluvial systems (Mosselman et al., 2000; Rinaldi et al., 2008; Kleinhans, 2010) and event-based, graded sediment simulations reproducing reach-scale morphodynamics of natural rivers are beginning to emerge (Williams et al., 2016b). Moreover, such models have been used to shed light on how the morphodynamics of braided rivers are influenced by sediment heterogeneity (Sun et al., 2015; Singh et al., 2017) and vegetation (Crosato and Saleh, 2011; Li and Millar, 2011; Nicholas et al., 2013a; Iwasaki et al., 2017). Despite this progress, mesoscale physics-based simulations require considerable computational resource and can diverge from predicting feasible morphology (Schuurman et al., 2015). Beyond this classic dichotomy, a third approach to morphodynamic simulation draws on particle-based methods from granular physics (Frey and Church, 2012). This approach is however, computationally intensive and the absence of appropriate upscaling methods limits its application to patch-scale investigations of sediment entrainment, transport and deposition (e.g., Escauriaza and Sotiropoulos, 2011; Nabi et al., 2013).

25

The lack of morphodynamic modelling approaches that are optimized effectively for use at the mesoscale presents the opportunity for an alternative framework. An attractive approach is to couple flow routing predictions based upon the well-understood and robust shallow water wave equations (Nicholas et al., 2012; Williams et al., 2013) with a simplified, empirically-derived rule set for sediment transport, which in turn is used to update the bed topography. This schema has the advantage of decoupling the fastest components of the system (the hydrodynamics) from the slowest (evolution of the bed). Furthermore, an approach to sediment transport modelling

30



based on particle path lengths, the characteristic distance travelled by sediment particles during a flood (Davy and Lague, 2009; Furbish et al., 2016), has potential to simplify simulation of bedload transport representing the fundamental process that leads to bar formation and morphodynamics. Recent work indicates that morphology, bed structure, and texture play a key role in particle dispersion (Hassan and Bradley, 2017). Particle path length distributions have been found to take several forms in gravel-bed braided rivers, including exponential decay, or heavy-tailed distributions, marked by a large number of particles mobilized short distances downstream, resulting from floods that do not generate sufficient shear stress for transport across the braidplain width (Pyrce and Ashmore, 2003b). During floods which are competent across large areas of the braidplain, typical path length distributions exhibit peaks which correspond to the location of likely depositional sites downstream. Kasprak et al. (2015) and Pyrcce and Ashmore (2003a,b) both noted that these depositional sites were most frequently the location of bar heads (e.g. flow diffluences) and as such, particle path length distributions could be readily constructed using morphometric indices that reflect the characteristic confluence-diffluence spacing.

This paper presents a new, hybrid morphodynamic modelling approach that employs two-dimensional CFD hydraulics resolved at the event scale and a rule-set for sediment transport that leverages hydraulic predictions to determine particle path lengths along which to erode and route sediment and subsequently evolve topography. Previous research on particle path length distributions has largely been conducted in gravel-bed braided rivers, and as such the model described here, termed MoRPHEd (Model of Riverine Physical Habitat and Ecogeomorphic Dynamics), has been developed for such environments. Characteristic particle travel distances have, however, also been documented for single-thread channels (Pyrce and Ashmore, 2003b), so it may therefore be possible to apply the underlying theory to a wide variety of channel forms. That said, the approach is only appropriate where the extremes of the path length distribution are less than the length of the system to be modelled (i.e. for gravel- rather than sand-bed rivers).

Combining both dynamical (force-based hydraulics) and kinematic (motion-based prediction of particle transport) frameworks provides an effective compromise that incorporates the necessary physics to simulate the key driving forces and vectors of motion, but offers simultaneously a reduced complexity structure suitable for wide-area, long-term morphodynamic modelling. This paper explores the degree to which MoRPHEd (a) can capture the emergent properties of natural fluvial environments, (b) can maintain, but not necessarily form or produce, braided topography, and (c) exhibits sensitivity to contrasting process representations.



For transparency and ease of future development, the model presented here has been packaged into an open source code published at <https://github.com/morphed/MoRPHEd> and a user interface (<https://github.com/morphed/MoRPHEd-Viewer>). The novel contributions set out in this paper are: (i) a new, numerical morphodynamic modelling framework that combines a dynamics-based, CFD approach to predicting flow routing and a kinematics-based, particle travel length rule set for sediment transport and morphological change; (ii) testing the modelling framework using data from two contrasting natural rivers, with sensitivity analyses to assess hydrograph discretization strategies and path length statistical distributions; and (iii) multi-scalar model verification using a plurality of rigorous validation approaches including reach-scale quantitative morphological change budgets and the pattern of contribution of different braiding mechanisms.

10

## 2 The Model

As with many previously-developed morphodynamic models, the model used here (MoRPHEd v. 1.1) simulates hydraulics and uses these calculations to predict bedload transport and morphological change. This section details the methods used in each of these components, along with ancillary routines such as the parameterization of model boundaries, sediment grain size, and bank erosion. Fig. 1 shows a flowchart of model operation along with required/optional inputs and outputs; these components are discussed throughout this section.

15

[INSERT FIGURE 1 NEAR HERE]

### 2.1 Hydraulics

20

The model's hydraulic component is driven using the freely-available, open-source Delft3D software (Version 4.00.01). Delft3D solves the shallow-water form of the Navier-Stokes equations, which relate changes in momentum (left-hand terms) in time and space to the cumulative surface and body forces acting on the fluid (right-hand terms).

25

$$\rho \left( u \frac{\partial u}{\partial x} + v \frac{\partial u}{\partial y} \right) = -\frac{\partial P}{\partial x} + \mu \left( \frac{\partial^2 u}{\partial x^2} + \frac{\partial^2 u}{\partial y^2} \right) [1]$$

$$\rho \left( u \frac{\partial v}{\partial x} + v \frac{\partial v}{\partial y} \right) = -\frac{\partial P}{\partial y} + \mu \left( \frac{\partial^2 v}{\partial x^2} + \frac{\partial^2 v}{\partial y^2} \right) [2]$$



Where  $x$  and  $y$ , respectively, denote the streamwise and cross-stream directions of velocity ( $u, v$ ),  $P$  denotes pressure forces on a body of fluid,  $\rho$  is fluid density, and  $\mu$  denotes dynamic viscosity. We employed the model in depth-averaged form (i.e., two-dimensional) as this provided an ideal compromise between computational efficiency and the ability to resolve hydraulics at the cellular scale of our DEMs (Lane et al., 1999). Although Delft3D three-dimensional flow simulations have been applied in river environments (e.g. Parsapour-Moghaddam and Rennie, 2017), the parameterization, validation, and computational overhead associated with three-dimensional modelling precludes their use for the development and assessment of MoRPHEd (Lane et al., 1999; Brasington and Richards, 2007). For all modelling, we employed fixed Cartesian orthogonal grids which were generated using the RGFRID module of the Delft3D software suite. The model time step was then adjusted to satisfy the Courant-Friedrichs-  
5  
10 Levy condition to ensure computational stability of the solution.

For all simulations, discharge was specified at the upstream boundary and a corresponding water surface elevation was set at the downstream boundary, and was calculated using a normal depth approximation based on reach-average slope and roughness. Horizontal eddy viscosity ( $\nu$ ) was set at  $0.1 \text{ s/m}^2$  (Williams et al., 2013). A spatially  
15 constant bed roughness was used, based on the Colebrook-White equation to determine the 2D Chezy coefficient:

$$C_{2D} = 18 \log_{10} \frac{12H}{k_s} \quad [3]$$

where  $H$  is water depth and  $k_s$  is the Nikuradse roughness length, which can be described in terms of a factor ( $\alpha_x$ )  
20 of the characteristic grain diameter as:

$$k_s = \alpha_x D_{84} \quad [4]$$

Here, we used  $D_{84}$  as the characteristic grain size as it provides an estimate of coarse grain influence on the flow  
25 field. Using grain size distribution available for both of the modelling sites used in this paper (Hodge et al., 2009; Williams et al., 2013), we computed  $k_s$  using  $\alpha_x$  of 2.9, taken as the averaged from a range of gravel-bed rivers studied in Garcia (2006). This resulted in values of  $k_s = 0.1$  and  $0.29$  for the Rees River and River Feshie respectively.



Models were run with a steady upstream discharge, corresponding to the peak of a flood and hydraulic predictions were extracted for further sediment transport calculations only once the reach had achieved steady state (no observed change in depth, velocity, or inundation). This approach was adopted because: (a) the calculation of morphodynamics at coarser time intervals allows for greatly reduced computational overhead associated with the model; and (b) modelling at finer timescales, while allowing the ability to capture rapid transient events such as prograding bedload sheets and bank retreat during the course of a single flood, is inherently difficult given that the most common observational data are channel form before and after a single event (Bertoldi et al., 2010; Williams et al., 2011; Mueller et al., 2014), and sediment transport distances resulting from that event (Pyrce and Ashmore, 2003a,b; Snyder et al., 2009; Kasprak et al., 2015). The exception to this approach is documented in Sect. 4.2.1, in which the hydrograph of a single flood event was schematized as a set of three steady discharges corresponding to the rising limb, peak, and falling limb of the event. This schematization was used in an attempt to evaluate the need for quasi-dynamic flow predictions to capture distinct stage-specific morphodynamic processes, such as the dissection of bar-top chutes at falling stages (e.g. Wheaton et al., 2013), and because sediment transport capacity may change throughout a hydrograph as supply is exhausted (e.g. hysteresis in the sediment rating curve; Topping et al., 2007). From each hydraulic simulation we exported: (a) water depth; (b) flow velocity resolved into streamwise and lateral components; and (c) bed shear stress.

## 2.2 Bed Sediment Erosion

The model employs a critical nondimensional value of the bed shear stress (Shields stress) to determine whether sediment can be entrained at a particular location. The theory and threshold values of Shields stress for entrainment have been well studied in gravel-bed river settings. Incipient motion for gravel occurs when the Shields stress ( $\tau_*$ ) exceeds 0.03-0.07 (Buffington and Montgomery, 1997; Snyder et al., 2009):

$$\tau_* = \frac{\tau_B}{(\rho_s - \rho)gD} \quad [5]$$

where  $\rho_s$  is a characteristic sediment density (2650 kg/m<sup>3</sup>),  $g$  is acceleration due to gravity, and  $D$  is the median particle size. The spatial distribution of local bed shear stress ( $\tau_B$ ) at steady flow was computed using Delft3D and the critical Shields stress for sediment mobility was set at 0.05. The modelled bed shear varies significantly over small spatial regions (Wilcock et al., 2009) and could therefore, lead to large cell-to-cell variability in elevation



change and unstable coupling of the bed topography and modelled hydraulics. To avoid such effects, the local  $\tau_B$  was averaged along a streamline derived from the Delft3D-output velocity vectors, taking the 10 cells upstream and downstream of the cell in question. Although lateral averaging of shear stress could additionally reinforce model stability, this was not explored here. The result is a single average value of bed shear stress that is used for computation of scour depth at each cell.

Most morphodynamic models compute bed elevation change using some form of the Exner equation for sediment continuity (Paola and Voller, 2005). In this, bed elevation ( $z$ ) through time ( $t$ ) is a function of the sediment supplied from upstream ( $V_s$ ), the divergence of the sediment flux through the reach boundaries ( $Q_s$ ) and the porosity of the deposited sediment ( $\gamma_p$ ).

$$\frac{\partial z}{\partial t} = \frac{1}{1-\gamma_p} \left( \frac{\partial V_s}{\partial t} + \nabla \cdot Q_s \right) \quad [6]$$

To ensure computational stability, morphodynamics are typically computed by solving Eq. (6) at fine time steps (seconds-minutes) using solutions from the equations of motion. However, MoRPHEd is designed specifically to operate on long timesteps, reflecting the timescales of integrated sediment transport pathways. As such, we used an alternative approach to local sediment continuity equation, based on Montgomery et al. (1996), who derived a theoretical relationship to predict event-scale sediment scour depth ( $D_s$ ):

$$D_s = \frac{Q_b}{u_b \rho_s (1-\gamma)} \quad [7]$$

where  $Q_b$  is the average bedload transport rate during the event,  $u_b$  is the bedload velocity, and  $\gamma$  is the bed sediment porosity. While estimates of  $Q_b$  are present a continuing challenge, here we adopt the well-known Meyer-Peter Müeller (1949) formulation, which relates transport to excess shear stress which can be readily extracted from the Delft3D simulations:

$$Q_b = (\tau_B - \tau_{BC})^{1.5} \quad [8]$$

and  $u_b$ , the bedload velocity, can be estimated as:



$$u_b = a(u_* - u_{*c}) \quad [9]$$

where  $u_*$ , the shear velocity, is computed as:

5

$$u_* = \sqrt{\frac{\tau_b}{\rho}} \quad [10]$$

The constant  $a$  in Eq. (9) has been studied by many researchers (Garcia, 2006), but is generally accepted to take a value close to 9. Although the accuracy of using Eq. (7) to predict event-scale scour depth has not been explored empirically, it represents one of the few methods for predicting the depth of scour over extended durations and is intended to be used here in a largely exploratory manner.

10

### 2.3. Bank Sediment Erosion

Readily-erodible banks are a hallmark of braided rivers (Wheaton et al., 2013) yet continue to represent one the most difficult geomorphic processes to represent numerically (Darby and Thorne, 1996; Simon et al., 2000; Rinaldi and Darby, 2007; Stecca et al., 2017). Most existing models rely on fine timesteps and detailed predictions of the near bank force balance to predict bank stability. As MoRPHEd is a simplified event-scale model, here we estimate the lateral retreat distance by empirically scaling near-bank shear stress and bank slope to the distance of lateral retreat during a model run.

15

To begin, the model calculates the slope of all cells in the model domain; all simulations presented herein used a cell resolution of 2 m (Rees River; Sect. 3.1) or 1 m (River Feshie; Sect. 3.2). The relatively coarser cell resolution on the Rees was chosen for computational efficiency, particularly with regard to the hydraulic modelling component of MoRPHEd, as the Rees site encompassed a considerably larger spatial domain than that of the Feshie. Cells that exceed a user-defined slope criterion, which was empirically calibrated to 7% for all simulations presented herein (Fig. 2.1), are then identified. Whether bank erosion occurs by mass failure or lateral channel migration, eroding banks are often marked by steep slopes, and as such this criterion was used as the first metric for computing bank sediment erosion. This slope delineation produces groups of cells, which are removed from the selection if the group's area falls below a user-specified threshold (Fig. 2.2). Here, we set this threshold area to 30 cells, again adjusting this value to mirror the size of field-observed bank erosion patches; we also observed that

20

25

30



very small area thresholds would create discontinuous patches of lateral retreat, leading to model instability and hydraulic artefacts in subsequent runs. The bed shear stress in the surrounding cells is then sampled using a 3 x 5 neighbourhood window and each cell within this neighbourhood that exceeds the critical shear value for the grain size in that cell is noted (Fig. 2.3). The bed shear stress values in these cells are averaged, producing a single shear stress value for the delineated group of cells. Those cell groups with average shear stress below a user-defined criteria, here set to 50 N/m<sup>2</sup>, are excluded. For each remaining group of cells, the model removes material from a number of cells specified by Eq. (10), which computes the lateral extent of bank erosion ( $n$ ), rounded to the nearest whole cell, as a function of slope ( $S$ ) and near-bank shear stress ( $\tau$ ; Fig. 2.4):

$$n = \text{round}\left(\left(\frac{\tau}{3} + 1\right) * \frac{S}{15}\right) \quad [11]$$

Material is removed from cells working in a direction opposite the bank cells' aspect (Fig. 2.4). Eroded cells are reduced in elevation to a level equal to that of the lowest cell in the initial neighbourhood surrounding the bank cell (sensu Nicholas, 2013), and eroded sediment is immediately transported downstream and deposited in a manner identical to that described, below, for bed transport and deposition.

[INSERT FIGURE 2 NEAR HERE]

## 2.4 Bed/Bank Sediment Transport and Deposition

Once entrained, bed or bank sediment is mobilized downstream along flowlines which are delineated using velocity vectors from Delft3D. Although the model is inherently a cell-based (e.g. raster) model, velocity vectors need not pass through the centre of each cell. Instead, the absolute coordinate of each velocity vector is calculated at a downstream interval equal to the computational domain cell size. In the field, deposition of sediment consistently occurs in diffuse patterns, such as 'tear-drop' forms of lobate bars, prograding bedload sheets, and thinly-mantled overbank deposits (Ashmore, 1982; Ferguson and Werritty, 1983; Wheaton et al., 2013). To mirror this diffuse deposition, the model distributes sediment within a 5x5 window of cells surrounding the candidate deposition cell, with the candidate cell receiving 1/3 of the deposited sediment, the adjacent eight cells receiving 1/3 of the deposited sediment between them, and the outer ring of 16 cells receiving the final 1/3 of deposited sediment. In



the case of dry cells that occur in the 5x5 neighbourhood, the dry cell(s) sediment is divided among the population of wetted cells in the neighbourhood.

At each cell along the flowpath, the volume of sediment to deposit in the centre cell is given by a path length distribution (Fig. 3). In the simplest sense, this distribution details the proportion of all eroded sediment which is deposited at a particular distance downstream, and provide a representation of field-mapped source-sink pathways found in braided rivers (Williams et al., 2015). These distributions have been studied by numerous researchers and found to take several forms in braided rivers, as reviewed in Sect. 1. MoRPHED deposits a proportion of the path-length specified volume of sediment in each wetted cell of the 5x5 neighbourhood described above. Path-length distributions in the model can take typical field-measured forms (Gaussian and Exponential Decay; Pyrcce and Ashmore, 2003b), or can take any user-specified form (e.g. multi-peaked), as specified by an input text file.

[INSERT FIGURE 3 NEAR HERE]

## 15 2.5 Sediment Import and Export

For each simulated event, the model tracks the volume of sediment passing the downstream or lateral reach boundaries. In effect, export of sediment occurs when the length of the user-specified path length distribution exceeds the downstream or lateral boundaries of the model domain. When this occurs, the remaining volume of sediment (the amount of eroded sediment not yet deposited along the flowline) is recorded as having been exported from the reach. Sediment import is user-specified and can be (a) set equal to the volume of sediment export during the preceding event (e.g. sediment equilibrium; Grams and Schmidt, 2005), (b) specified as a percent of sediment export during the preceding event, or (c) specified via a text file detailing absolute volumetric sediment import during each event (e.g. sedigraph timeseries). Algorithmically, the model computes flowpaths from each wetted cell at the upstream reach boundary and distributes the total volume of imported sediment to each cell of each flowpath as specified in the user-input path length distribution.

## 2.6 Grain Size and Stratigraphy

30 The model dynamically tracks the median particle size ( $D_{50}$ ) in each model cell for each simulated event. The routine used for grain size averaging is similar to that employed by Viparelli et al. (2010). The model domain is



initially divided into a series of layers (Fig. 4) extending upward from the lowest point in the initial DEM. The active, or surface, layer may vary from cell to cell with variations in elevation, and is tracked from event to event. All layers have a constant, user-defined thickness ( $Z_{LYR}$ ) except the active layer, which may take any thickness ( $Z_{ACT}$ ) such that:

5

$$0 < Z_{ACT} < Z_{LYR} \quad [12]$$

With regard to tracking changes in  $D_{50}$  at the event scale, the simplest case is that of erosion at a cell. The new grain size in that cell ( $D_{NEW}$ ) is simply the grain size given by the corresponding layer at the cell's new elevation (following scour):

10

$$D_{NEW} = D_{LYR} \quad [13]$$

The sediment size of the scoured material ( $D_{ERODED}$ ) is computed as either the grain size of active layer at the eroded cell (provided scour did not extend through the active layer) or as a weighted average of the eroded material (if the scour did extend through the active layer and into subsurface layers):

15

$$D_{ERODED} = \begin{cases} D_{ACT}, & \text{if } Z_{ERODED} \leq Z_{ACT} \\ \sum \frac{D_i Z_i}{Z_{ERODED}}, & \text{else} \end{cases} \quad [14]$$

The calculation of grain size changes due to deposition takes place at the conclusion of an event's model run. The grain size of all sediment that has been deposited in a particular cell is either averaged with the grain size of the active layer (as in Eq. (14), if the amount of deposition does not require the addition of a new active layer), or is divided into as many new layers as are necessary given the user-defined layer thickness, each of which is assigned the averaged grain size of the deposited sediment. Note that while this routine may be used for the computation of grain size and stratigraphy at a particular cell, all model runs described here employed a single representative grain size across the model reach.

25

[INSERT FIGURE 4 NEAR HERE]

## 2.7 Model Verification

30



To compare the outputs of the model with field-based surveys of channel evolution, we derived several morphometric parameters along with comparing DEMs-of-Difference (DoDs) and contributions of individual braiding mechanisms to total geomorphic change. Each of these three verification components are discussed below.

### 5 2.7.1 Morphometric Indices

We manually quantified braiding index ( $I_B$ ) for the initial and final field surveys and model runs of each simulation described here. Braiding index was computed by averaging the number of channels across five evenly spaced transects along the length of the model domain (Howard et al., 1970; Egozi and Ashmore, 2008). Channels were  
10 defined by wetted areas as modelled using Delft3D at estimated baseflow for each modelling site. In addition, we measured the mode, or total sinuosity ( $S_T$ ) of the modelled reach for the first and last model runs in each system. Total sinuosity (Richards, 1982) was defined by the ratio of the length of all anabranches ( $L_A$ ) compared to the down-valley length of the model domain ( $L_D$ ):

15 
$$S_T = \frac{L_A}{L_D} \quad [15]$$

Finally, we computed the number of confluences, diffluences, and channel heads for initial and final field and model DEMs. The procedure for delineating confluences, diffluences, and channel heads is detailed by Wheaton et al. (2013). In brief, it requires manual location of areas where one anabranch splits into two anabranches (a  
20 diffluence), areas where two anabranches join to form one anabranch (a confluence), and locations where small side channels or chutes begin (a channel head). In theory, the number of confluences should be roughly equal to the number of diffluences plus the number of channel heads for a braided river; large differences in this metric are indicative of distributary systems (e.g. deltas; Jerolmack and Morhig, 2007) or dendritic networks that collect low order channels into a few main channels.

25

### 2.7.2 DEMs-of-Difference

We differenced DEMs of initial and final field surveys and model simulations using Geomorphic Change Detection software (version 6, <http://gcd.joewheaton.org>; Wheaton et al., 2010). Differencing DEMs from two survey periods  
30 produces a DEM-of-Difference (DoD), or a map of geomorphic changes that occurred during the inter-survey



period. While the DEM differencing process is straightforward, accounting for error in the resultant DoD is necessary as each constituent DEM contains an inherent level of error (that may vary on a cell-by-cell basis), which can ultimately influence the estimated magnitude of geomorphic change in the DoD. Here we modelled DEM error using the most straightforward of the available approaches: we simply assumed that each of the constituent DEMs contained no error and computed the DoD. We then thresholded, or removed areas of change, from the DoD if they were less than  $\pm 0.1$  m in magnitude (herein termed the 'minimum level of detection' or minLoD). For decadal-scale modelling and field surveys on the River Feshie, we employed a threshold of  $\pm 0.2$  m to better visualize and delineate braiding mechanisms and to account for the larger magnitude elevation changes that occurred over wide swaths of the braidplain over this extended timescale. While this simple thresholding method is not necessarily the most robust available for modelling error in field-surveyed DEMs, those DEMs output from the model do not contain survey error as would be expected from field-based DEMs. As such, a simple minLoD of 0.10 m allowed us to use identical error modelling methods to directly compare areas of change in field and modelled DoDs while simultaneously removing a great deal of the survey noise/uncertainty present in field DEMs, along with removing extremely low-magnitude elevation changes in modelled DEMs.

15

From DoDs, we extracted elevation change distributions (a histogram of all volumetric changes), along with deriving the net sediment imbalance during each survey and model period (the percent departure of the sediment budget from equilibrium conditions).

### 20 **2.7.3 Braiding Mechanisms**

Using GCD software, we mechanistically segregated thresholded DoDs by delineating the processes responsible for each area of geomorphic change (Ashmore, 1991; Wheaton et al., 2013). These processes can be separated into four 'braiding mechanisms' described by Ashmore (1991): central bar development, lobe dissection, transverse bar dissection, and chute cutoff. To these, Wheaton et al. (2013) added an additional six mechanisms that are not unique to braided rivers: bank erosion, channel incision (i.e. bed erosion), overbank sheets, confluence pool scour, bar trimming, and lateral bar development. Hereafter, these ten processes are referred to simply as 'braiding mechanisms'. We mapped the areas in DoDs where each of these mechanisms occurred; areas where we could not confidently assign a mechanism of change were classified as questionable or unresolved change. This classification allowed us to compute and compare the volumetric contribution of each braiding mechanism to total geomorphic change in both field and model-derived DoDs.

30



### 3 Study Sites

#### 3.1 Rees River, South Island, New Zealand - Event and Annual Scales

5

The braided gravel bedded Rees (Fig. 5) drains a 402 km<sup>2</sup> catchment of the uplifting metasedimentary Southern Alps and flows into Lake Wakitipu. The 2.5 km study reach is an actively braided channel which flows through a deglaciated valley, and the river is braiding in response to sediment delivery from the tectonically-active landscape (Williams et al., 2013). The hydrology of the system is dominated by response to glacial melt and storms, and undergoes floods in the spring, summer, and fall that may completely alter the morphology of the braidplain over the course of a single flood. A temporary gauging station at Invincible (6 km upstream of the study reach) operated from 2009-2011 and is used to drive hydraulic components of the model. Mean discharge during the 2010 and 2011 hydrological years was 20 m<sup>3</sup>s<sup>-1</sup>, with a maximum flow of 475 m<sup>3</sup>s<sup>-1</sup> (Williams et al., 2015). The survey data on the Rees include 0.5 m digital elevation models (DEMs) constructed via a fusion of terrestrial laser scanning (TLS) and optical-empirical bathymetric mapping surveys (Williams et al., 2014), which were downsampled to 2 m resolution for modelling. In total, ten floods ranging from 51 m<sup>3</sup>s<sup>-1</sup> to 403 m<sup>3</sup>s<sup>-1</sup> were captured as part of the ReesScan project (Brasington et al., 2012) from 2009-2011, with post-flood DEMs surveyed in the period between each high flow. These pre- and post-flood DEMs, along with a continuous hydrologic record and a high degree of dynamism across the braidplain at the event scale, make the Rees an ideal candidate to examine the performance of the model at the event and annual scales.

20

#### 3.2 River Feshie, Scotland - Annual and Decadal Scales

The weakly-braided gravel bedded Feshie (Fig. 5) is a tributary of the Spey River and drains 231 km<sup>2</sup> of mountainous, postglacial terrain. Underlain by metamorphic and igneous rocks, the basin ranges from 230 m - 1260 m in elevation. The mean flow near the river's outlet was reported by Ferguson and Werritty (1983) as 8 m<sup>3</sup>s<sup>-1</sup> with  $Q_5 = 80 \text{ m}^3\text{s}^{-1}$ . Topographic data for the 1 km study reach of the Feshie consist of nine years of resurveys (2000, 2002-2008, 2013) comprising more than a decade of channel change using RTK-GPS (2000-2006) along with TLS and RTK-GPS fusion scans performed for three surveys (2007-8, 2013). DEMs generated from field surveys on the Feshie had a cell resolution of 1 m. Additionally, the Feshie dataset contains continuous hydrograph data (~55 years) and aerial photo records (~60 years), along with UK Ordnance Survey channel planform maps dating to

30



1869. The Feshie has been the site of a great deal of previous research ranging from bar morphodynamics (Ferguson and Werritty, 1983; Wheaton et al., 2013) to development of riverine survey and DEM-differencing/change detection methodologies (Brasington et al., 2007; Vericat et al., 2007; Hodge et al., 2009; Wheaton et al., 2010). The combination of annual resurveys capturing over a decade of channel change in combination with mapping and  
5 aerial photographs dating back over a century make the Feshie an ideal candidate to examine the performance of the model at the annual and decadal scales. In addition, the Feshie site provides a mechanistic contrast to the Rees in that overall flood-to-flood dynamism is reduced via vegetation cohesion and fine sediment (Ferguson and Werritty, 1983), and the dominant mechanisms of change vary from those seen on the Rees, particularly with regard to chute cutoff and bank erosion (Wheaton et al., 2013).

10

[INSERT FIGURE 5 NEAR HERE]

## 4 Results

### 15 4.1 Hydraulic Model Calibration

#### 4.1.1 Rees River

The outputs of Delft3D on the Rees (depth, velocity, inundation extent) were compared with field-surveyed values  
20 across a range of discharges and used to calibrate the model parameters (Colebrook-White roughness and horizontal eddy viscosity) until good agreement was reached. The reader is referred to Williams et al. (2013) for more detailed analysis of the validity of Delft3D on the Rees (and in braided gravel-bed rivers in general). In short, here we used the same upstream and downstream boundaries, as well as grid resolution, as Williams et al. (2013), keeping both  $k_s$  (0.10) and  $\nu$  (0.10) constant in line with their results (Table 1).

25

#### 4.1.2 River Feshie

In contrast to the Rees, no comprehensive calibration and verification of Delft3D exists on the Feshie; as such, we leveraged existing surveys of wetted areas from 2003-2007 in concert with surveyed water depth in those years to  
30 examine the performance of Delft3D. Because field surveys were conducted at low flows to facilitate rapid measurement of braidplain topography, here we are only able to verify the results of Delft3D at these low flows.



However, Delft3D has been employed and verified on gravel-bed braided rivers at flood stage (Javernick, 2013), demonstrating that the model can accurately reproduce flood-stage hydraulic features and can be used to drive morphodynamic evolution at the event-scale. For modelling on the Feshie, we estimated discharge by downscaling the average observed flow for the relevant survey period at the nearest gauging station (SEPA No. 8013, Feshie at Feshiebridge) located approximately 11 km downstream, using an empirically-derived discharge-area coefficient of 0.71 (Wheaton et al., 2013). The value of discharge taken at Feshiebridge was the average flow during each year's survey period (average of two weeks). We estimated the downstream water elevation using surveyed inundation extent in combination with the DEM for each year modelled. Downstream water surface elevation estimated from the spatial data were cross-checked using a reach-scale conveyance calculation (Williams et al., 2013).

Results of our calibration of Delft3D on the Feshie at low flow are shown in Fig. 6. Here we report (a) the mean of depth differences between modelled and observed values ( $D_{diff}$ ), along with (b) the congruence of the modelled and measured inundation extents ( $F_c$ ; Bates and De Roo, 2000) as described by the ratio of intersection and union areal extents. These two metrics are described by Eqs. (16-17), respectively.

$$D_{diff} = \frac{\sum_{i=1}^n x_{mod} - x_{obs}}{n} \quad [16]$$

$$F_c = \frac{IA_{obs} \cap IA_{mod}}{IA_{obs} \cup IA_{mod}} * 100 \quad [17]$$

The metrics indicate that at low flow, Delft3D accurately predicted both depth and inundation extent across the Feshie study reach. Both  $D_{diff}$  and  $F_c$  are consistent with values obtained by Williams et al. (2013) on the Rees, and are indicative of good agreement between hydraulic predictions and field-observed flow characteristics, despite the empirically scaled discharge.

[INSERT FIGURE 6 NEAR HERE]

25

#### 4.2 Event-Scale Morphodynamic Modelling: Rees River

We modelled a single flood event on the Rees River that occurred between 8-16 December 2009 as the result of heavy rainfall in the upstream watershed (Fig. 7). Peak flows reached a maximum instantaneous discharge of 259  $m^3s^{-1}$  at the upstream Invincible gauging station during the afternoon of 9 December. Two smaller peaks in the

30



hydrograph of  $75 \text{ m}^3\text{s}^{-1}$  (afternoon of 8 December and morning of 12 December) also occurred during this event. Our modelling employed a single representative grain size ( $D_{50}$ ) of 20 mm. Geomorphic change captured by pre- and post-flood terrestrial laser scanning revealed that the most volumetrically significant mechanisms of change were transverse bar conversion (22%), bank erosion (21%), and lobe dissection (19%). Qualitatively, event-scale dynamics across the study reach are marked by widespread geomorphic change, particularly in the centre of the braidplain where development of a single main channel occurred via channel incision, bank erosion, and avulsions of smaller anabranches leading to deposition and subsequent dissection of mid-channel bars. Geomorphic change on the edges of the braidplain was somewhat muted, consisting largely of infilling of anabranches and accretion of central bars. Field-surveyed elevation changes ranged from -1.70 m to +1.32 m (Fig. 7D). The braiding index ( $I_B$ ) decreased from 3.6 to 2.0 following the flood, and total sinuosity ( $S_T$ ) decreased from 4.5 to 2.9.

[INSERT FIGURE 7 NEAR HERE]

Results of morphodynamic modelling on the Rees for this event are shown in Fig. 7. Total model runtime for the single event was approximately 90 minutes. Modelled elevation changes in the study reach ranged from -1.76 m to +0.89 m (Fig. 7E). Overall, geomorphic change was concentrated near the centre of the braidplain, similar to geomorphic change measured from field data. Large swaths of bank erosion along a central anabranch developed, although not to the extent seen in field data. In general, geomorphic change in the modelled DoD appears muted in comparison to the field-based DoD. This is reflected in the elevation change distribution (ECD) shown for field and model data on the Rees (Fig. 7C), particularly with regard to the erosional component of volumetric change ( $47,598 \text{ m}^3$  in the field compared to  $20,663 \text{ m}^3$  in the model; Table 2). Similarly, depositional volumes were greater in the field ( $35,551 \text{ m}^3$ ) compared to those in the model ( $16,188 \text{ m}^3$ ; Table 2). Average magnitudes of erosion and deposition agree well between field and model results. On average, erosion depth across the study reach was 0.13 m as observed through field measurement, and 0.07 m when modelled. Deposition averaged 0.10 m in the field and 0.06 m in the model (Table 2). The most volumetrically-significant braiding mechanisms in this run were central bar development (25% of total volumetric change), bar edge trimming (16%), and bank erosion (15%).

[INSERT TABLE 2 NEAR HERE]

#### 4.2.1 Case Study: Hydrograph Discretization



The choice of model timestep is one of the more important considerations in morphodynamic modelling, whereby the user must strike the optimal balance between a model timestep fine enough to preserve computational stability, yet which is coarse enough to allow computation over meaningful timescales (Brasington et al., 2007). To investigate the implications of altering the model timestep in MoRPHEd, we discretized the hydrograph used in event-scale modelling on the Rees (Sect. 4.2.1) so as to model three discrete points over the course of the modelled flood (Fig. 8). These discharges were 75, 254, and 75 m<sup>3</sup>s<sup>-1</sup>, respectively. Planform DoD, ECD, and volumetric contribution of individual braiding mechanisms from this discretized model run are shown in Fig. 8. In general, morphologic changes were more widespread across the braidplain in the case of the discretized hydrograph modelling run than the single peak discharge hydrograph (Fig. 8), with overall area of change increasing, yet still smaller than field-observed change volumes (157,504 m<sup>2</sup> in the model compared to 287,184 m<sup>2</sup> in field data; Table 2). The ECD from this model run more closely approximated the field-derived ECD, with low-magnitude elevation changes (e.g. < 1 m) dominating the change distribution (Fig. 8).

[INSERT FIGURE 8 NEAR HERE]

15

### 4.3 Annual-Scale Morphodynamic Modelling: River Feshie

We modelled morphodynamics during the one-year period from July 2003 to July 2004 on the Feshie. The estimated hydrograph for the study reach, based on the empirical downscaling coefficient applied to the Feshiebridge gauge (Sect. 3.2) during this period is shown in Fig. 9A. This survey epoch contained 16 flood peaks above the 'low bankfull' discharge estimate (20 m<sup>3</sup>s<sup>-1</sup>; Ferguson and Werritty, 1983) at the study reach; these are denoted in Fig. 9 and were used as model inputs. While the use of bankfull discharge as an estimate of flow competence is simplistic, we use this threshold for two reasons: (a) Wheaton et al. (2013) noted that the number of flow peaks in excess of bankfull discharge in any year was related to the amount of geomorphic change over a period of five years, and (b) Ashworth and Ferguson (1989) documented that flows of 20 m<sup>3</sup>s<sup>-1</sup> were indeed competent for bed material in the study reach, albeit without full mobility of all bed particle sizes. As such, the use of a low bankfull estimate for competence provides an easily measured threshold for competent flows that we know is related to geomorphic change in the study reach. Our modelling on the Feshie employed a single representative grain size ( $D_{50}$ ) of 50 mm.

30

[INSERT FIGURE 9 NEAR HERE]



Wheaton et al. (2013) noted that the most volumetrically significant braiding mechanisms during the 2003-2004 period were chute cutoff (29%), bank erosion (16%), and channel incision (15%). Overall geomorphic change was primarily confined to a main channel bisecting the braidplain longitudinally, with one anabranch on the left side of the braidplain undergoing bank erosion and central bar development. Braiding index ( $I_B$ ) during the 2003-2004 epoch increased from 1.8 to 2.8, and total sinuosity ( $S_T$ ) also increased from 2.5 to 3.5. Results of morphodynamic modelling are shown in Fig. 9E. Total model runtime for the series of 12 events modelled during the 2003-2004 period was approximately 6 hours. The results of DEM differencing are shown in Table 3. Elevation changes in the modelled reach ranged from -1.25 m to +1.49 m. Overall geomorphic change was marked by the accumulation of transverse bars and the development of central bars throughout the model reach, along with incision of a central anabranch. Sculpting or trimming of central bars (Fig. 9F; e.g. Wheaton et al., 2013) was also prevalent. The most volumetrically-significant braiding mechanisms during this model run were channel incision (26%), transverse bar conversion (20%), and central bar development (14%). Overall, geomorphic change predicted via modelling was greater than that observed from field data (Table 3). However, both field and model ECDs (Figs. 9B, 9C) depict change distributions wherein the greatest volume of geomorphic change is the result of low-magnitude elevation changes. The average depth of elevation changes were generally well predicted by the model, although average erosion and deposition depths were over-estimated by 0.02 and 0.03 m, respectively (Table 3).

[INSERT TABLE 3 NEAR HERE]

20

#### 4.3.1 Case Study: Contrasting Path-Length Distributions

Transport and deposition of eroded bed or bank sediment in MoRPHEd is a function of the path length distribution used in the model. While field or laboratory data describing particle transport distances can be used to produce a path length distribution, parameterizing such a distribution for sites where tracer data are not available is not straightforward. Here we employed average confluence-difffluence spacing to estimate the peak of the distribution (Fig. 3; Pyrce and Ashmore, 2003a,b; Kasprak et al., 2015). To further understand the effect of contrasting path length distribution shapes and distances, we used MoRPHEd to model the annual hydrograph on the River Feshie in a manner identical to Sect. 4.3, except we varied the characteristics of the specified path length distribution (Fig. 10). We employed a compressed Gaussian distribution (Fig. 10A), a flattened Gaussian distribution (Fig. 10B), and an exponential decay-type distribution (Fig. 10C; Pyrce and Ashmore, 2003b); each of these distributions had a

30



total length identical to our original distribution on the Feshie (Fig. 10A). We also modelled two shortened distributions (length = 50 m): a shortened Gaussian distribution (Fig. 10D) and a shortened exponential distribution (Fig. 10E).

5 [INSERT FIGURE 10 NEAR HERE]

Overall, the geomorphic changes predicted by the model were strikingly similar at the reach scale, and areas of scour and deposition generally aligned between all five of the simulations (Figs. 10A - 10E). Analysis of the elevation change distribution produced using each path length distribution revealed that while the compressed and stretched Gaussian distributions were marked by more laterally-extensive deposition at higher magnitudes (e.g. ~1 m), the exponential and two shortened distributions (Figs. 10C - 10E) generally contained depositional signatures marked by numerous low-magnitude (e.g.  $\Delta z < 0.5$  m) changes. The same is true for the erosional component of elevation change, with compressed and stretched Gaussian distributions marked by a wide range of erosional elevation changes up to and exceeding 1 m, whereas the exponential and shortened distributions generally displayed erosional changes less than -1 m in elevation.

#### 4.4 Decadal-Scale Morphodynamic Modelling: River Feshie

We modelled morphodynamics during the ten-year period between July 2003 and June 2013 along the River Feshie. The estimated hydrograph at Glen Feshie during this period is shown in Fig. 11A, and we modelled all peaks above the low bankfull discharge as described in Sect. 3.2 and in Wheaton et al. (2013), for a total of 185 flood events ranging from  $20 \text{ m}^3\text{s}^{-1}$  to  $95 \text{ m}^3\text{s}^{-1}$ .

Differencing DEMs from survey data at the beginning and end of the analysis period reveals elevation changes ranging from -2.4 m to +2.1 m (Fig. 11D). DEM differencing indicates that the study reach underwent slight net aggradation (+3.6% imbalance). The most volumetrically significant braiding mechanisms during this time period were the development of central bars (25% of volumetric changes), transverse bar conversion (17%), and bank erosion (16%). As the relative contribution of individual braiding mechanisms may be misleading at decadal scales due to signature overprinting and hence difficulty in interpretation of braiding mechanism (Collins et al., 2012), we note that over a 5-year period (2003-2007; Wheaton et al., 2013) on the Feshie, the most volumetrically significant braiding mechanisms were chute cutoff (24%), bank erosion (20%), and transverse bar conversion



(19%). Braiding index ( $I_B$ ) during the 2003-2013 epoch increased from 1.8 to 2.4, and total sinuosity ( $S_T$ ) also increased from 2.5 to 2.9 (Fig. 11).

Results of morphodynamic modelling from 2003-2014 are shown in Fig. 11E. Total model runtime for the 185-  
5 flood series was approximately 72 hours. Geomorphic change ranged from +2.1 m to -8.07 m (Fig. 11E). A mask  
was employed to exclude areas of the reach < 25 m from the upstream boundary, as boundary artefacts resulting  
from the use of point discharges in the Delft3D model produced high magnitudes of geomorphic change (e.g., > 5  
m) in these areas. While geomorphic change in the field was marked by generally thin-mantled erosion and  
deposition across the braidplain, the model produced more widespread, high-magnitude erosional change (Table  
10 4). While the ECD produced by the model generally characterized the form of the field-derived ECD (Figs. 11B,  
11C), the model predicted a smaller area, but greater volume, of scour (Table 4). The model generally reproduced  
the form and magnitudes of deposition seen in the field, but the lowest-magnitude deposition (e.g. < 0.5 m) was  
more volumetrically significant in the field than in the model. In particular, the model did not produce avulsions  
seen in the field, but rather predicted continued downcutting of the central anabranch seen in the 2003 DEM. The  
15 most volumetrically-significant braiding mechanisms during the 2003-2013 model run were central bar  
development (27%), transverse bar conversion (22%), and lobe dissection (1%). In addition, the role of bar edge  
trimming (8%), a process treated identically to bank erosion in MoRPHEd, was magnified compared to field-  
derived mechanistic segregation (2%), as was the role of channel incision (11% in the model as compared to 7%  
in the field).

20

[INSERT FIGURE 11 AND TABLE 4 NEAR HERE]

## 5 Discussion

25 We developed a morphodynamic model that computes sediment transport according to user-specified path length  
distributions, and subsequently employed this model to predict channel evolution at two braided river reaches  
across timescales ranging from a single event to a decade. We observed that the model reproduced many of the  
geomorphic changes observed in the field, although the magnitude and mechanisms of those changes often diverged  
from observations using field data. At the same time, the modular design of the modelling framework may hold  
30 promise for exploration of braided channel evolution, and also raises questions regarding the way processes are  
represented algorithmically and the model's sensitivity to those process representations.



## 5.1 Emergent versus parameterized processes

Braided rivers undergo geomorphic change as a result of numerous morphodynamic processes, or braiding  
5 mechanisms (Ashmore, 1991; Wheaton et al., 2013; Kasprak et al., 2015). Given its highly simplified nature, the  
degree to which these braiding mechanisms must be explicitly represented as algorithms in morphodynamic  
modelling deserves exploration. Of the ten braiding mechanisms discussed in Sect. 2.7.3, the model produced eight  
simply as a result of the bed erosion, transport, and deposition functions included in the model. Only bank erosion  
and bar edge trimming required the inclusion of a lateral channel migration component. As the surfaces undergoing  
10 bank erosion and bar edge trimming are not necessarily submerged during a flood, these processes cannot be  
captured simply by an excess shear stress scour approach (Eq. (7); Sect. 2.2).

The geomorphic changes that the model most commonly produces are those that result from focused scour and  
longitudinally-continuous deposition, given the nature of the scour and deposition functions used in the model. In  
15 particular, channel incision, bar edge trimming, bank erosion, and lateral/central bar development are common  
processes produced by the model (Figs. 7, 9, 11). Additionally, given the single-peaked Gaussian distributions  
used herein, those braiding mechanisms which involve deposition immediately downstream of an erosional source  
are difficult to reproduce. For example, Wheaton et al. (2013) demonstrated the importance of chute cutoff as a  
braiding mechanism on the Feshie, noting that chute development across point bars not only manifested as erosion,  
20 but that the scoured material was often deposited immediately downstream of the chute. Similarly, scoured bank  
material (e.g. mass failures) may often be deposited at the bank toe rather than transported downstream. In both  
cases, the model makes no differentiation in transporting the eroded sediment, mobilizing the material according  
to the user-specified path-length distribution; as such, proximal couplets of erosion and deposition are difficult to  
reproduce in the model. Finally, we note that chute cutoff in the model always occurred in locations of pre-existing  
25 chutes across point bars. Because chute cutoff often occurs at the falling stage of floods, when braidplain-inundating  
flows are first being confined into anabranches, our model may not properly reproduce chute cutoff as a result of  
only computing peak flood hydraulics, and averaging shear stress across a range of model cells. Although headward  
erosion of these pre-existing chutes typically occurred in the model, thus increasing their extent, we did not observe  
any instances where chute cutoff was initiated in the model without an existing chute or channel head being present  
30 on a bar surface. As such, chute cutoff may represent a braiding mechanism that must be explicitly included in the  
model's code in order to be properly represented in the future.



## 5.2 Sensitivity to process representation

### 5.2.1 Hydrograph discretization

5

In Sect. 4.2.1, we modelled a single event on the Rees as three discrete discharges on the hydrograph (Fig. 8). Because MoRPHEd under-predicted the volume of change, particularly due to the absence of low-magnitude scour, during the single-event simulation (Fig. 7), we sought to understand whether discretizing the hydrograph would allow for an improved prediction of overall volumetric change, and low-magnitude erosional change in particular.

10 Overall, discretizing the hydrograph into three modelling timesteps only marginally increased predictions of volumetric change across the study reach: total volumetric change in the discretized run (Fig. 8) was 39,771 m<sup>3</sup>, compared to 36,851 m<sup>3</sup> in the single-event model run (Fig. 7). It might appear counterintuitive that discretizing the hydrograph and running the model three times would not appreciably increase the amount of volumetric change. We believe the reason for this is that in many cases, deposition offsets erosion, particularly in inundated areas,  
15 leading to little net increase in volumetric change despite running the model multiple times. The exception to this is in areas that experience bank erosion or avulsions, where high-magnitude scour may occur in areas which are not inundated, thereby producing locations where deposition does not counteract scour. Both modelling approaches underestimated the amount of volumetric change in the field (83,149 m<sup>3</sup>).

20 Discretizing the hydrograph also increased the amount of low-magnitude scour predicted by the model (Fig. 8B), more accurately reflecting the field-derived elevation change distribution (Fig. 7B). It is likely that this is the result of the 0.1 m elevation thresholding used in our change detection (Sect. 2.7.2), whereby additive changes due to erosion largely did not exceed 0.1 m depth after a single flood event, but did exceed this threshold when three discrete hydrograph points were measured. Whereas erosional processes that lead to high-magnitude scour, such  
25 as bank erosion, dominated the elevation change distribution in the single-event model run, processes such as channel incision and lobe dissection were more prevalent in the discretized hydrograph model run. Additionally, several areas of high-magnitude bank and bar trimming were largely offset by deposition of imported or scoured material during the discretized hydrograph run, thereby decreasing the overall magnitude of scour in those areas (Fig. 8B).

30

### 5.2.2 Path length distribution



We modelled annual-scale morphodynamics on the Feshie using five different path length distributions (Sect. 4.3.1). The similarity between the DEMs produced by the model (and hence, the DoDs shown in Fig. 10) using these distributions is striking, yet subtle differences may reflect the distinct nature of the spatial arrangement of erosion and deposition. Overall, the similarity between the modelled distributions may also be the result of the smoothing algorithms used in the model to ensure computationally-stable output surfaces, such as the along-flow averaging of shear stress and neighbourhood windows used for deposition (Sect. 2.4), both of which may act to reduce the variability introduced by the choice of a particular path length distribution.

In fluvial settings, erosional processes typically operate over small spatial scales (e.g. bank erosion, bar trimming, pool scour), and the magnitude of scour in these focused areas is typically higher than diffuse, broad-scale depositional processes such as overbank sheets or accretion of mid-channel or lateral bar material (Wheaton et al., 2013). As such, we suggest that the overall similarities, as well as the differences between our model's outputs using these contrasting path length distributions reflects the ability of deposition to counterbalance elevation changes due to scour of material, and the fact that the diffuse nature of the path length distributions used here make this counterbalancing difficult. For example, the compressed and stretched Gaussian distributions (Figs. 10A, 10B) are both marked by broad areas of erosion and deposition typically falling between  $\pm 1$  m in elevation change. However, high-magnitude areas of erosion are more rare, yet still present, in the stretched Gaussian distribution, which may be due to the more longitudinally-extensive deposition of scoured material partially offsetting elevation changes due to erosion. The compressed and stretched Gaussian distributions stand in contrast to the exponential and shortened distributions (Figs. 10C - 10E), where elevation changes are largely confined between  $\pm 0.5$  m, and overall are more fragmented across the model reach. This does not reflect a reduced magnitude of erosion, as Eq. (7) was used in all cases to predict scour depth; rather, the fragmented nature of elevation changes, along with the narrower range of those changes, is likely due to the propensity for deposition to offset erosional changes given the more focused nature of the path length distributions in Figs. 10C - 10E. Nevertheless, in all distributions used, the volume of material deposited in a given cell following erosion upstream is always a fraction of that which was eroded. Using the distributions in Fig. 10 and the deposition smoothing window detailed in Sect. 2.4, the volume of sediment deposited falls between 0.4% and 8% of the volume which is eroded, and as such, erosion may outpace deposition in many cells.

30

### 5.2.3 Imperfect models as exploratory tools



Models in the Earth sciences are necessarily imperfect (Oreskes et al., 1994), and the highly simplified nature of MoRPHEd, combined with the highly dynamic and nonlinear nature of braided river morphodynamics (Ashmore, 1991; Bristow and Best, 1993) implies that our model will necessarily fail to achieve perfect replication of field-  
5 observed geomorphic dynamics. However, even imperfect models can provide meaningful insight into the processes behind morphologic evolution of fluvial systems (Paola et al., 2009; Paola and Voller, 2009). MoRPHEd is designed to facilitate experimentation, particularly with regard to process inclusion or the particular aspects of process representation of bed and bank erosion, transport, deposition, and import dynamics (Fig. 1). For example, in Sect. 4.3.1, we explored the implications of altering the path-length distributions for bed and bank sediment  
10 transport/deposition, along with seeking to understand the advantages and drawbacks of discretizing hydrographs during model runs. The notion of morphodynamic modelling that employs sediment transport routines based on particle path length distributions is in its infancy, and we have built the model as an exploratory tool that can be used to investigate the utility of this approach toward predictive modelling of braided river evolution. Several components of the model may be employed to investigate longstanding questions in our understanding of braided  
15 river dynamics, starting with the path-length approach itself. Recent field-based research on braided rivers has confirmed the coupled nature of sediment sources and sinks and the influence of sediment pathways on braiding maintenance (Williams et al., 2015). While it has long been hypothesized, and field and laboratory data have often confirmed, that mobilized particles in braided rivers are preferentially deposited in association with regularly-occurring channel bars (e.g. Pyrcce and Ashmore, 2003a,b; Kasprak et al., 2015), the form of the path length  
20 distribution, and its relationship to geomorphic unit spacing, is deserving of further study across braided systems. As such, the choice of path length distribution and subsequent comparison of model results with field observations may provide insight into the applicability of path length distributions on a system-by-system basis (Hassan et al., 2013).

25 MoRPHEd may also be used to investigate the utility of event-scale monitoring. Existing morphodynamic models typically employ a sediment continuity approach (e.g. Exner; Eq. (6), operating at very fine temporal scales, typically seconds to minutes. This approach produces results consistent with field observation (Bates et al., 2005), but comes at the expense of computational overhead, thereby restricting the timescales that can be modelled (Brasington et al., 2007). Because the timestep of the model is, by default, a single event, computational resources  
30 are conserved, allowing for extended simulations at annual and decadal timescales. However, it is unclear whether processes that occur over the course of a competent flow (e.g. avulsions, bank failures) can be adequately captured



using an event-scale modelling approach. Similarly, the degree to which a hydrograph may need to be discretized and its constituent parts modelled (Sect. 4.2.1) to capture stage dependent processes such as the development of chute cutoffs or bar edge trimming (Wheaton et al., 2013) is deserving of further investigation.

5 Our exploratory research into decadal-scale modelling on the River Feshie (Sect. 4.4) indicates that both the accurate prediction of event-scale scour depth, and subsequent deposition location, present methodological hurdles in the development of valid morphodynamic models that operate at the timescale of competent flows. In our model, as in the field, erosion occurs in discrete, focused areas of high magnitude (e.g. pool scour, bar trimming, bank retreat; Ashmore, 1991; Bristow and Best, 2003; Wheaton et al., 2013). Deposition occurs thinly over more broad  
10 spatial areas (e.g. bedload sheets, overbank sheets, bar formation), a result of the path length distributions employed here and the smoothing required to avoid the generation of rough topography that would lead to hydraulic instability. One result of the differences in the nature of erosion and deposition is that deposition may never 'catch up' to erosion if a simple path-length distribution is employed, thus resulting in over-scouring of channels (Fig. 11). In general, the morphodynamic signature of deposition mirrors that seen in the field (see ECDs in Figs. 7, 9, 11),  
15 with a large contribution of total change coming from areas of shallow deposition. However, in future event-scale morphodynamic models, it may be necessary to augment path length distributions so as to preferentially deposit material in certain geomorphic units (e.g. confluence pools, deep channels adjacent to banks) in order to develop lateral flow, bank material removal, and channel migration/avulsion (Ashmore, 1991).

20 Another process that is difficult to capture algorithmically is the lateral retreat of banks. Highly erodible banks are a hallmark of braided rivers and lead to the development of central bars and multiple anabranches (Ashmore, 1991). However, the Cartesian grid employed in the model, along with the event-scale timestep of the model, makes the generation of smooth bank features difficult. While approaches are available that compute bank stability based on a factor-of-safety approach that balances downslope gravitational forces with the ability of bank material to provide  
25 cohesive resistance to failure (Darby and Thorne, 1996; Simon et al., 2000; Rinaldi and Darby, 2007), parameterization of these models, especially at the reach scale, is quite difficult. The simplified approach employed in the model averages the slope of bank cells and the near-bank shear stress of the flow to predict bank retreat distances (Sect. 2.3). The threshold slope and shear stress, and their effect on lateral retreat distance, have been empirically adjusted to emulate field-observed bank dynamics. We have observed that the simple treatment of  
30 lateral erosion in the model produces bank erosion and bar edge trimming. However, whether this simplified approach will provide computational stability over longer-term (e.g. centennial) simulations is unknown.



Additionally, further investigation is needed to determine whether the inclusion of bank toe deposition, as opposed to immediate downstream transport according to a user-specified path length distribution, is necessary in the model, along with whether bank material should be transported and deposited according to the same path-length distribution as was used for bed material.

5

## 6 Conclusions

The morphodynamic model developed here simulates braided river evolution at a variety of timescales via a path-length based approach, and here we applied the model to two braided river reaches at the event, annual, and decadal scale. The premise of MoRPHEd is that sediment transport can be approximated using path length distributions (Pyrce and Ashmore, 2003a,b; Kasprak et al., 2015), which, when coupled with two-dimensional hydraulic simulations at peak flood discharge, results in decreased computational overhead, thus enabling longer simulations at improved spatial resolution. We observed overall correspondence between model outputs and field observations when comparing planform changes, geomorphic change described by elevation change distributions, and morphometric indices such as sinuosity, braiding index, and channel node counts (Sect. 2.7.1). At the same time, divergence between field and model datasets was evident, suggesting that a purely path-length-based approach may oversimplify the highly dynamic nature of braided systems (Bristow and Best, 1993). Specifically, at event scales on the Rees River, New Zealand, we observed under-prediction of areal and volumetric changes (total areal extent of change in the field was 287,184 m<sup>2</sup> compared to 142,547 m<sup>2</sup> in the model, total volumetric change was 83,149 m<sup>3</sup> in the field and 36,851 m<sup>3</sup> in the model). At annual timescales on the River Feshie, UK, the model over-predicted the extent and volume of geomorphic change (areal extent of change was 17,206 m<sup>2</sup> in the field versus 37,707 m<sup>2</sup> in the model, volumetric changes were 4,349 m<sup>3</sup> in the field and 10,149 m<sup>3</sup> in the model). When conducting decadal-scale modelling on the Feshie over the period from 2003-2013, we observed good correspondence between areal and volumetric predictions of deposition (areal extent of deposition was 36,045 m<sup>2</sup> in the field compared to 26,861 m<sup>2</sup> in the model, volumetric deposition was 14,677 m<sup>3</sup> in the field and 13,748 m<sup>3</sup> in the model) and the areal extent of erosion (23,836 m<sup>2</sup> in the field compared to 23,542 m<sup>2</sup> in the model), but the model overpredicted the volume of erosion throughout the reach (12,680 m<sup>3</sup> in the field compared to 23,744 m<sup>3</sup> in the model).

While we did observe reproduction of all field-observed braiding mechanisms (Wheaton et al., 2013), the relative contribution of these mechanisms often varied from values seen in the field. In contrast to all other braiding mechanisms, neither bank erosion nor bar edge trimming emerged simply as a result of bed scour and deposition,

30



and instead needed to be explicitly parameterized in the model. In addition, chute cutoff only occurred at areas where pre-existing chutes or channel heads were observed, and did not appear to emerge across previously flat bar tops. While this model represents a first step in event-scale, path-length-based morphodynamic modelling, further testing is needed to evaluate the feasibility of the approach for longer-term modelling runs and/or for determination of whether process representation that accounts for inter-flood geomorphic change, such as avulsions or bank mass failure (Leddy et al., 1993; Ashworth et al., 2004) will require explicit parameterization. We have designed the model to be a modular framework for exploring the effect of various process representations, and as a learning tool designed to reveal the relative importance of geomorphic transport processes in braided river dynamics at multiple timescales.

10

**Data Availability:** All model code used in this manuscript can be found at <https://github.com/morphed/MoRPHEd>.

**Competing Interests:** The authors declare that they have no competing interests.

15

**Acknowledgements:** This research was supported by a grant from the National Science Foundation (No. 1147942). We thank Philip Bailey (North Arrow Research) for extensive assistance with model code and algorithm development. Field work on the Feshie was completed with the generous permission of Thomas MacDowell and the Glenfeshie Estate, with the assistance of Niall Lehane (Queen Mary University of London), Mark Smith (University of Leeds), Julian Leyland (Southampton University), and Damiá Vericat (Forest Technology Institute of Catalunya). Our modelling efforts benefited from substantial discussion with Sara Bangen, Nate Hough-Snee, Wally MacFarlane, Eric Wall, and Peter Wilcock (Utah State University), along with Rebecca Hodge (Durham University) and David Sear (Southampton University). Any use of trade, product, or firm names is for descriptive purposes only and does not imply endorsement by the U.S. Government.

25



## References

- Ashmore, P.E.: Laboratory modelling of gravel braided stream morphology, *Earth Surf. Proc. Land.*, 7, 201-225, doi: 10.1002/esp.3290070301, 1982.
- Ashmore, P.E.: How do gravel-bed rivers braid, *Can J. Earth Sci.*, 28, 326-341, doi: 10.1139/e91-030, 1991.
- 5 Ashworth, P.J., Best, J.L., and Jones, M.A.: Relationship between sediment supply and avulsion frequency in braided rivers, *Geology*, 32, 21-24, doi: 10.1130/g19919.1, 1994.
- Ashworth, P.J., and Ferguson, R.I.: Size-selective entrainment of bed load in gravel bed streams, *Water Resour. Res.*, 25, 627-634, doi: 10.1029/wr025i004p00627, 1989.
- Bates, P. and De Roo, A.: A simple raster-based model for flood inundation simulation, *J. Hydrol.*, 236, 54-77, doi: 10.1016/s0022-1694(00)00278-x, 2000.
- 10 Bates, P.D., Lane, S.N., and Ferguson, R.I. (Eds.): *Computational Fluid Dynamics*, John Wiley and Sons, Chichester, UK, 2005.
- Belletti, B., Rinaldi, M., Bussettini, M., Comiti, F., Gurnell, A.M., Mao, L., Nardi, L., and Vezza, P.: Characterising physical habitats and fluvial hydromorphology: a new system for the survey and classification of river geomorphic units, *Geomorphology*, 283, 143-157, doi: 10.1016/j.geomorph.2017.01.032, 2017.
- 15 Bertoldi, W., Zanoni, L., and Tubino, M.: Assessment of morphological changes induced by flow and flood pulses in a gravel bed braided river: the Tagliamento River (Italy), *Geomorphology*, 114, 348-360, doi: 10.1016/j.geomorph.2009.07.017, 2010.
- Black, E., Renshaw, C., Magilligan, F., Kaste, J., Dade, W., and Landis, J.: Determining lateral migration rates of meandering rivers using fallout radionuclides, *Geomorphology*, 123, 364-369, doi: 20 10.1016/j.geomorph.2010.08.004, 2010.
- Brasington, J. and Richards, K.: Reduced-complexity, physically-based geomorphological modelling for catchment and river management, *Geomorphology*, 90, 171-177, doi: 10.1016/j.geomorph.2006.10.028, 2007.
- Brasington, J., Vericat, D., and Rychkov, I.: Modelling river bed morphology, roughness, and surface sedimentology using high resolution terrestrial laser scanning, *Water Resour. Res.*, 48, W11519, doi: 25 10.1029/2012wr012223, 2012.
- Brasington J., Wheaton, J.M., Vericat, D., and Hodge, R.: Modelling braided river morphodynamics with terrestrial laser scanning, AGU Fall Meeting, San Francisco, California, 10-14 December, 2007.
- Bristow, C. and Best, J.: *Braided rivers: perspectives and problems*, Geological Society, London, UK, 1993.



- Buffington, J.M. and Montgomery, D.R.: A systematic analysis of eight decades of incipient motion studies, with special reference to gravel-bedded rivers, *Water Resour. Res.*, 33, 1993-2029, doi: 10.1029/97wr03138, 1997.
- Coulthard, T. and Van De Wiel, M.: Modelling river history and evolution, *Physical and Engineering Sciences*, 5 370, 2123-2142, doi: 10.1098/rsta.2011.0597, 2012.
- Coulthard, T.M., Macklin, M., and Kirkby, M.: A cellular model of Holocene upland river basin and alluvial fan evolution, *Earth Surf. Proc. Land.*, 27, 269-288, doi: <http://dx.doi.org/10.1002/esp.318>, 2002.
- Crosato, A. and Saleh, M.S.: Numerical study on the effects of floodplain vegetation on river planform style, *Earth Surf. Proc. Land.*, 36, 711-720, doi: 10.1002/esp.2088, 2011.
- 10 Crowder, D. and Diplas, P.: Using two-dimensional hydrodynamic models at scales of ecological importance, *J. Hydrol.*, 230, 172-191, doi: 10.1002/esp.318, 2000.
- Darby S. and Thorne, C.: Development and testing of riverbank-stability analysis, *J. Hydraul. Eng.*, 122, 443-454, doi: 10.1061/(ASCE)0733-9429(1996)122:8(443), 1996.
- Davy, P. and Lague, D.: Fluvial erosion/transport equation of landscape evolution models revisited, *J. Geophys. Res-Earth*, 114, F03007, 2009.
- 15 Egozi R. and Ashmore, P.E.: Experimental analysis of braided channel pattern response to increased discharge, *J. Geophys. Res-Earth*, 114, F02012, doi: 10.1029/2008jf001099, 2009.
- Escauriaza, C. and Sotiropoulos, F.: Lagrangian model of bed-load transport in turbulent junction flows, *J. Fluid Mech.*, 666, 36-76, doi: 10.1017/S0022112010004192, 2011.
- 20 Ferguson, R.: Gravel-bed rivers at the reach scale, *Developments in Earth Surface Processes*, 11, 33-53, doi: 10.1016/s0928-2025(07)11112-3, 2007.
- Ferguson R. and Werritty, R.A.: Bar development and channel changes in the gravelly River Feshie, Scotland, *Modern and Ancient Fluvial Systems*, 181-193, doi: 10.1002/9781444303773.ch14, 1983.
- Frey, P. and Church, M.: Gravel Transport in Granular Perspective, in: *Gravel-Bed Rivers: Processes, Tools, Environments*, edited by M. Church, P. A. Biron and A. G. Roy, Wiley, Chichester, 37-55, 2012.
- 25 Furbish, D.J., Schmeeckle, M.W., Schumer, R., and Fathel, S.L.: Probability distributions of bed load particle velocities, accelerations, hop distances, and travel times informed by Jaynes's principle of maximum entropy, *J. Geophys. Res-Earth*, 121, 1373-1390, doi: 10.1002/2016JF003833, 2016.
- Garcia, M.H.: *Sedimentation Engineering*, American Society of Civil Engineers, Reston, Virginia, 2006.



- Grams, P.R. and Schmidt, J.C.: Equilibrium or indeterminate? Where sediment budgets fail: sediment mass balance and adjustment of channel form, Green River downstream from Flaming Gorge Dam, Utah and Colorado, *Geomorphology*, 71, 156-181, doi: 10.1016/j.geomorph.2004.10.012, 2005.
- Gurnell, A., Surian, N., and Zanoni, L.: Multi-thread river channels: A perspective on changing European alpine river systems, *Aquat. Sci.*, 71, 253-265, doi: 10.1007/s00027-009-9186-2, 2009.
- Hassan, M.A., Voepel, R., Schumer, G., Parker, G., and Fraccarollo, L.: Displacement characteristics of coarse fluvial bed sediment, *J. Geophys. Res-Earth*, 118, 155-165, doi: 10.1029/2012jf002374, 2013.
- Hassan, M.A. and Bradley, D.N.: Geomorphic Controls on Tracer Particle Dispersion in Gravel-Bed Rivers, in: *Gravel-Bed Rivers: Processes and Disasters*, edited by D. Tsutsumi and J. Laronne, Wiley, Chichester, UK, 159-184, 2017.
- Hodge, R., Brasington, J., and Richards, K.: In situ characterization of grain-scale fluvial morphology using Terrestrial Laser Scanning, *Earth Surf. Proc. Land.*, 34, 954-968, doi: 10.1002/esp.1780, 2009.
- Hooke, J.: River channel adjustment to meander cutoffs on the River Bollin and River Dane, northwest England, *Geomorphology*, 14, 235-253, doi: 10.1016/0169-555x(95)00110-q, 1995.
- Howard, A.D., Keetch, M., and Linwood, V.C.: Topological and geometrical properties of braided streams, *Water Resour. Res.*, 1674-1688, doi: 10.1029/wr006i006p01674, 1970.
- Iwasaki, T., Shimizu, Y., and Kimura, I.: Numerical simulation of bar and bank erosion in a vegetated floodplain: a case study in the Otofuke River, *Adv. Water Resour.*, 93, 118-134, doi: 10.1016/j.advwatres.2015.02.001, 2017.
- Javernick, L.A.: Modelling flood-induced processes causing Russell lupin mortality in the braided Ahuriri River, New Zealand, Ph.D. Dissertation, University of Canterbury, Christchurch, New Zealand, 2013.
- Jerolmack, D.J. and Mohrig, D.: Conditions for branching in depositional rivers, *Geology*, 35, 463-466, doi: 10.1130/g23308a.1, 2007.
- Kasprak A., Ashmore, P.E., Hensleigh, J., Peirce, S., and Wheaton, J.M.: The relationship between particle travel distance and channel morphology: results from physical models of braided rivers, *J. Geophys. Res-Earth*, 120, 55-74, doi: 10.1002/2014jf003310, 2015.
- Kleinbans, M.G.: Sorting out river channel patterns, *Prog. Phys. Geog.*, 34, 287-326, doi: 10.1177/0309133310365300, 2010.
- Kondolf, G., Piegay, H., and Landon, L.: Channel response to increased and decreased bedload supply from land use change: contrasts between two catchments, *Geomorphology*, 45, 35-51, doi: 10.1016/s0169-555x(01)00188-x, 2002.



- Lallias-Tacon, S., Liébault, F., and Piégay, H.: Step by step error assessment in braided river sediment budget using airborne LiDAR data, *Geomorphology*, 214, 307-323, doi: 10.1016/j.geomorph.2014.02.014, 2014.
- Lane S., Bradbrook, K., Richards, K., Biron, P., and Roy, A.: The application of computational fluid dynamics to natural river channels: three-dimensional versus two-dimensional approaches, *Geomorphology*, 29, 1-20, doi: 10.1016/s0169-555x(99)00003-3, 1999.
- 5 Leddy, J.O., Ashworth, P.J., and Best, J.L.: Mechanisms of anabranch avulsion within gravel-bed braided rivers: observations from a scaled physical model, in: *Braided Rivers*, Best, J.L. and Bristow, C.S. (eds.), Geological Society of London, London, UK, 1993.
- Li, S.S. and Millar, R.G.: A two-dimensional morphodynamic model of gravel-bed river with floodplain vegetation, *Earth Surf. Proc. Land.*, 36, 190-202, doi: 10.1002/esp.2033, 2011.
- 10 Minns, C.K., Kelso, J.R., and Randall, R.G.: Detecting the response of fish to habitat alterations in freshwater ecosystems, *Can. J. Fish. Aquat. Sci.*, 53, 403-414, doi: 10.1139/f95-262, 1996.
- Montgomery, D.R., Buffington, J.M., Peterson, N.P., Schuett-Hames, D., and Quinn, T.P.: Stream-bed scour, egg burial depths, and the influence of salmonid spawning on bed surface mobility and embryo survival, *Can. J. Fish. Aquat. Sci.*, 53, 1061-1070, doi: 10.1139/cjfas-53-5-1061, 1996.
- 15 Mosselman, E., Shishikura, T., and Klaassen, G.: Effect of bank stabilization on bend scour in anabranches of braided rivers, *Phys. Chem. Earth*, 25, 699-704, doi: 10.1016/s1464-1909(00)00088-5, 2000.
- Mueller, E.R., Grams, P.E., Schmidt, J.C., Hazel, J.E., Alexander, S., and Kaplinski, M.: The influence of controlled floods on fine sediment storage in debris fan-affected canyons of the Colorado River Basin, *Geomorphology*, 226, 65-75, doi: 10.1016/j.geomorph.2014.07.029, 2014.
- 20 Murray, A.B. and Paola, C.: A cellular model of braided rivers, *Nature*, 371, 54-57, doi: 10.1038/371054a0, 1994.
- Nabi, M., de Vriend, H.J., Mosselman, E., Sloff, C.J., and Shimizu, Y.: Detailed simulation of morphodynamics: 2. Sediment pick-up, transport and deposition, *Water Resour. Res.*, 49, 4775-4791, doi: 10.1002/wrcr.20303, 2013.
- 25 Newson M. and Newson, C.: Geomorphology, ecology and river channel habitat: mesoscale approaches to basin-scale challenges, *Prog. Phys. Geog.*, 24, 195-217, doi: 10.1177/030913330002400203, 2000.
- Nicholas, A.P., Sandbach, S.D., Ashworth, P.J., Amsler, M.L., Best, J.L., Hardy, R.J., Lane, S.N., Orfeo, O., Parsons, D.R., Reesink, A.J.H., Sambrook-Smith, G.J., and Szupiany, R.N.: Modelling hydrodynamics in the Rio Paraná, Argentina: An evaluation and inter-comparison of reduced-complexity and physics based models applied to a large sand-bed river, *Geomorphology*, 169-170, 192-211, doi: 10.1016/j.geomorph.2012.05.014, 2012.
- 30



- Nicholas, A.P.: Modelling the continuum of river channel patterns, *Earth Surf. Proc. Land.*, 38, 1187-1196, doi: 10.1002/esp.3431, 2013a.
- Nicholas, A.P.: Morphodynamic modelling of rivers and floodplains, in: *Treatise on Geomorphology*, Wohl, E., (ed.), Academic Press, San Diego, 160–179, doi: 10.1016/B978-0-12-374739-6.00037-3, 2013b.
- 5 Nicholas, A. and Quine, T.: Crossing the divide: Representation of channels and processes in reduced-complexity river models at reach and landscape scales, *Geomorphology*, 90, 318-339, doi: 10.1016/j.geomorph.2006.10.026, 2007.
- Oreskes, N., Shrader-Frechette, K., and Belitz, K.: Verification, validation, and confirmation of numerical models in the Earth Sciences, *Science*, 253, 641-646, doi: 10.1126/science.263.5147.641, 1994.
- 10 Paola, C., Straub, K., Mohrig, D., and Reinhardt, L.: The 'unreasonable effectiveness' of stratigraphic and geomorphic experiments, *Earth Science Reviews*, 97, 1-43, doi: 10.1016/j.earscirev.2009.05.003, 2009.
- Paola, C. and Voller, V.: A generalized Exner equation for sediment mass balance, *J. Geophys. Res-Earth*, 110, doi: 10.1029/2004jf000274, 2005.
- Parsapour-Moghaddam, P. and Rennie, C.D.: Hydrostatic versus nonhydrostatic hydrodynamic modelling of secondary flow in a tortuously meandering river: Application of Delft3D, *River Research and Applications*, doi: 10.1002/rra.3214, 2017.
- 15 Pyrcce, R.S. and Ashmore, P.E.: Particle path length distributions in meandering gravel-bed streams: results from physical models, *Earth Surf. Proc. Land.*, 28, 951-966, doi: 10.1002/esp.498, 2003a.
- Pyrcce, R.S. and Ashmore, P.E.: The relation between particle path length distributions and channel morphology in gravel-bed streams: a synthesis, *Geomorphology*, 56, 167-187, doi: 10.1016/s0169-555x(03)00077-1, 2003b.
- 20 Richards, K.S.: *Rivers: Form and Processes in Alluvial Channels*, Blackburn Press, Methuen, Massachusetts, 1982.
- Rinaldi, M. and Darby, S.E.: Modelling river-bank-erosion processes and mass failure mechanisms: progress towards fully coupled simulations, in: *Gravel Bed Rivers VI - From Process Understanding to River Restoration*, Habsersack H., Piegay H., and Rinaldi, M. (Eds.), Elsevier, Netherlands, 213-219, 2007.
- 25 Rinaldi, M., Mengoni, B., Luppi, L., Darby, S.E., and Mosselman, E.: Numerical simulation of hydrodynamics and bank erosion in a river bend, *Water Resour. Res.*, 44, doi: 10.1029/2008wr007008, 2008.
- Rosenfeld, J.: Assessing the habitat requirements of stream fishes: an overview and evaluation of different approaches, *T. Am. Fish. Soc.*, 132, 953-968, doi: 10.1577/t01-126, 2003.



- Schuurman, F., Marra, W., and Kleinhans, M.: Physics-based modeling of large braided sand-bed rivers: Bar pattern formation, dynamics, and sensitivity, *J. Geophys. Res-Earth*, 118, 2509-2527, doi: 10.1002/2013JF002896, 2013.
- Schuurman, F.: Bar and channel evolution in meandering and braiding rivers using physics-based modelling, Ph.D. Dissertation, Utrecht University, Netherlands, 162 p, 2015.
- 5 Simon, A., Curini, A., Darby, S., and Langendoen, E.: Bank and near-bank processes in an incised channel, *Geomorphology*, 35, 193-217, doi: 10.1016/S0169-555X(00)00036-2, 2000.
- Singh, U., Crosato, A., Giri, S., and Hicks, M.: Sediment heterogeneity and mobility in the morphodynamic modelling of gravel-bed braided rivers, *Advances in Water Resources*, 104, 127-144, doi:10.1016/j.advwatres.2017.02.005, 2017.
- 10 Snyder, N.P., Castele, M.R., and Wright, J.R.: Bedload entrainment in low-gradient paraglacial coastal rivers of Maine, USA: Implications for habitat restoration, *Geomorphology*, 103, 430-446, doi: 10.1016/j.geomorph.2008.07.013, 2009.
- Stecca, G., Measures, R., and Hicks, D.M.: A framework for the analysis of noncohesive bank erosion algorithms in morphodynamic modelling, *Water Resour. Res.*, doi: 10.1002/2017WR020756, 2017.
- 15 Sun, J., Lin, B., and Yang, H.: Development and application of a braided river model with non-uniform sediment transport, *Advances in Water Resources*, 81, 62-74, doi: 10.1016/j.advwatres.2014.12.012, 2015.
- Thomas, R., Nicholas, A., and Quine, T.: Cellular modelling as a tool for interpreting historic braided river evolution, *Geomorphology*, 90, 302-317, doi: 10.1016/j.geomorph.2006.10.025, 2007.
- 20 Thomas, R. and Nicholas, A.: Simulation of braided river flow using a new cellular routing scheme. *Geomorphology*, 43, 179-195, doi: 10.1016/s0169-555x(01)00128-3, 2002.
- Topping D.J., Rubin, D.M., and Melis, T.: Coupled changes in sand grain size and sand transport driven by changes in the upstream supply of sand in the Colorado River: relative importance of changes in bed-sand grain size and bed-sand area, *Sediment. Geol.*, 202, 538-561, doi: 10.1016/j.sedgeo.2007.03.016, 2007.
- 25 Van De Wiel, M.J., Coulthard, T.J., Macklin, M.G., and Lewin, J.: Modelling the response of river systems to environmental change: Progress, problems and prospects for palaeo-environmental reconstructions, *Earth-Science Reviews*, 104, 167-185, doi: 10.1016/j.earscirev.2010.10.004, 2011.
- Vericat, D., Brasington, J., Wheaton, J., and Hodge, R.: Reach-Scale Retrieval of Alluvial Bed Roughness, AGU Fall Meeting, San Francisco, California, 10-14 December, 2007.



- Viparelli, E., Sequeiros, O.E., Cantelli, A., Wilcock, P.R., and Parker, G.: River morphodynamics with creation/consumption of grain size stratigraphy 2: numerical model, *Journal of Hydraulic Research*, 48, 727-741, doi: 10.1080/00221686.2010.526759, 2010.
- Wheaton, J.M., Brasington, J., Darby, S.E., and Sear, D.A.: Accounting for uncertainty in DEMs from repeat topographic surveys: improved sediment budgets, *Earth Surf. Proc. Land.*, 35, 136-156, doi: 10.1002/esp.1886, 2010.
- Wheaton, J.M., Brasington, J., Darby, S.E., Kasprak, A., Sear, D.A., and Vericat, D.: Morphodynamic signatures of braiding mechanisms as expressed through change in sediment storage in a gravel-bed river, *J. Geophys. Res-Earth*, 118, 759-779, doi: 10.1002/jgrf.20060, 2013.
- 10 Wilcock, P.R., Pitlick, J., and Cui, Y.: Sediment transport primer: estimating bed-material transport in gravel-bed rivers, USDA Forest Service Rocky Mountain Research Station, General Technical Report RMRS-GTR-226, 1-84, 2009.
- Wilcock, P.R. and Iverson, R.M.: *Prediction in Geomorphology*, Geophysical Monograph Series, American Geophysical Union Press, Washington, DC, doi: 10.1029/GM135, 2003.
- 15 Williams, R.D., Brasington, J., Hicks, M., Measures, R., Rennie, C., and Vericat, D.: Hydraulic validation of two-dimensional simulations of braided river flow with spatially continuous aDcp data, *Water Resour. Res.*, 49, 5183-5205, doi: 10.1002/wrcr.20391, 2013.
- Williams, R.D., Brasington, J., Vericat, D., Hicks, D.M., Labrosse, F., Neal, M.: Monitoring braided river change using terrestrial laser scanning and optical bathymetric mapping, in: *Geomorphological Mapping: Methods and Applications*, Smith M., Paron, P., and Griffiths, J. (eds.), Elsevier, Amsterdam, 507-532, 2011.
- 20 Williams, R.D., Rennie, C.D., Brasington, J., Hicks, D.M., and Vericat, D.: Linking the spatial distribution of bed load transport to morphological change during high-flow events in a shallow braided river, *J. Geophys. Res-Earth*, 120, 604-622, doi: 10.1002/2014JF003346, 2015.
- Williams, R.D., Brasington, J., and Hicks, D.M.: Numerical modelling of braided river morphodynamics: review and future challenges, *Geography Compass*, 10, 102-127, doi: 10.1111/gec3.12260, 2016a.
- 25 Williams, R.D., Measures, R., Hicks, D.M., and Brasington, J.: Assessment of a numerical model to reproduce event-scale erosion and deposition distributions in a braided river, *Water Resour. Res.*, doi: 10.1002/2015WR018491, 2016b.
- Ziliani, L., Surian, N., Coulthard, T.J., and Tarantola, S.: Reduced-complexity modelling of braided rivers: assessing model performance by sensitivity analysis, calibration and validation, *J. Geophys. Res-Earth*, 30 118, 2243-2262, doi: 10.1002/jgrf.20154, 2013.



5

10

## FIGURE CAPTIONS

**Figure 1.** MoRPHEd model operation flowchart

15

**Figure 2.** Lateral migration algorithm schematic

**Figure 3.** Path length distributions used in MoRPHEd modelling on (A) the River Feshie and (B) the Rees River. Peak of the distributions corresponds to average along-flow spacing between confluence and diffluence pairs.

20

**Figure 4.** MoRPHEd grain size and stratigraphy module. Top panel depicts model operation in the case of erosion, bottom panel depicts model operation during deposition.

**Figure 5.** Morphodynamic modelling sites. Overview maps of Rees River (left) and River Feshie (right). Hillshaded DEMs (2 m resolution for Rees and 1 m resolution for Feshie) are shown atop aerial photograph base. Information on data availability for both sites shown in lower panels.

25

**Figure 6.** River Feshie hydraulic modelling. Surveyed water surface extent in each of five years (2003-2007) was compared to modelled inundation extent in the same years using discharge levels approximated using data from gauge at Feshiebridge. Areas observed (but not predicted) to be inundated shown in blue, areas predicted (but not

30



observed) to be inundated shown in green. Areas which were correctly predicted as being inundated shown in red. Base is hillshaded 1 m DEM.

**Figure 7.** Rees River event morphodynamic modelling results. Continuous hydrograph and modelled discharge shown in (A). Elevation change distributions derived from field and model data shown in (B) and (C) respectively. DoD derived from field data shown in (D), with model-derived DoD and delineated braiding mechanisms shown in (E) and (F). Volumetric contributions of each braiding mechanism in field and modelled data shown in (G).

**Figure 8.** Rees River discretized hydrograph case study. DoD from MoRPHED modelling shown in (A), with ECD in (B) and event hydrograph with model points shown in (C). Refer to DoD and ECD in Figure 7 for comparison.

**Figure 9.** River Feshie annual morphodynamic modelling results. Refer to Figure 7 caption for details.

**Figure 10.** River Feshie variable path length case study. Path length distributions used are: compressed Gaussian (A), stretched Gaussian (B), and exponential (C), along with shortened Gaussian (D) and shortened exponential (E). DoDs for each path length distribution shown in middle row, with elevation change distributions shown in bottom row.

**Figure 11.** River Feshie decadal morphodynamic modelling results. Refer to Figure 7 caption for details. Note variable axes limits in (B) and (C).



**TABLE 1.** Delft3D hydraulic modelling parameters.

Site	Sim. Time (hrs)	Time Step (s)	Cell Size (m)	Nodes	$D_{50}$ (m)	W-C Roughness ( $k_s$ )	Eddy Viscosity ( $\nu$ , $\text{m}^2\text{s}^{-1}$ )
Rees	1	0.025	2	352,231	0.035	0.10	0.1
Feshie	1	0.025	1	201,116	0.1	0.29	0.1



**TABLE 2.** Rees River event modelling: geomorphic change detection results; results of discretized modelling shown in *italics*.

	<i>Field Raw</i>	<i>Field Thresholded (0.1 m)</i>	<i>MoRPHEd Raw</i>	<i>MoRPHEd Thresholded (0.1 m)</i>
<b>Areal</b>				
Total Area of Erosion (m <sup>2</sup> )	435,604	146,472	390,555 <i>418,856</i>	57,387 <i>63,496</i>
Total Area of Deposition (m <sup>2</sup> )	461,084	140,712	500,233 <i>389,072</i>	85,160 <i>94,008</i>
<b>Volumetric</b>				
Total Volume of Erosion (m <sup>3</sup> )	57,324	47,598	28,297 <i>28,679</i>	20,663 <i>20,291</i>
Total Volume of Deposition (m <sup>3</sup> )	47,022	35,551	28,102 <i>28,130</i>	16,188 <i>19,480</i>
<b>Vertical Averages</b>				
Average Depth of Erosion (m)	0.13	0.32	0.07 <i>0.07</i>	0.36 <i>0.32</i>
Average Depth of Deposition (m)	0.10	0.25	0.06 <i>0.07</i>	0.19 <i>0.21</i>
Average Total Thickness of Difference (m)	0.12	0.09	0.06 <i>0.07</i>	0.04 <i>0.05</i>
Average Net Thickness of Difference (m)	-0.01	-0.01	0.00 <i>0.00</i>	-0.01 <i>0.00</i>



**TABLE 3.** River Feshie annual modelling, geomorphic change detection results.

	<i>Field Raw</i>	<i>Field Thresholded (0.1 m)</i>	<i>MoRPHEd Raw</i>	<i>MoRPHEd Thresholded (0.1 m)</i>
<b>Areal</b>				
Total Area of Erosion (m <sup>2</sup> )	66,074	9,970	50,021	17,444
Total Area of Deposition (m <sup>2</sup> )	49,998	7,236	58,366	20,263
<b>Volumetric</b>				
Total Volume of Erosion (m <sup>3</sup> )	4,433	2,806	6,149	5,239
Total Volume of Deposition (m <sup>3</sup> )	2,704	1,543	5,986	4,910
<b>Vertical Averages</b>				
Average Depth of Erosion (m)	0.07	0.28	0.12	0.30
Average Depth of Deposition (m)	0.05	0.21	0.10	0.24
Average Total Thickness of Difference (m)	0.06	0.04	0.11	0.09
Average Net Thickness of Difference (m)	-0.01	-0.01	0.00	0.00

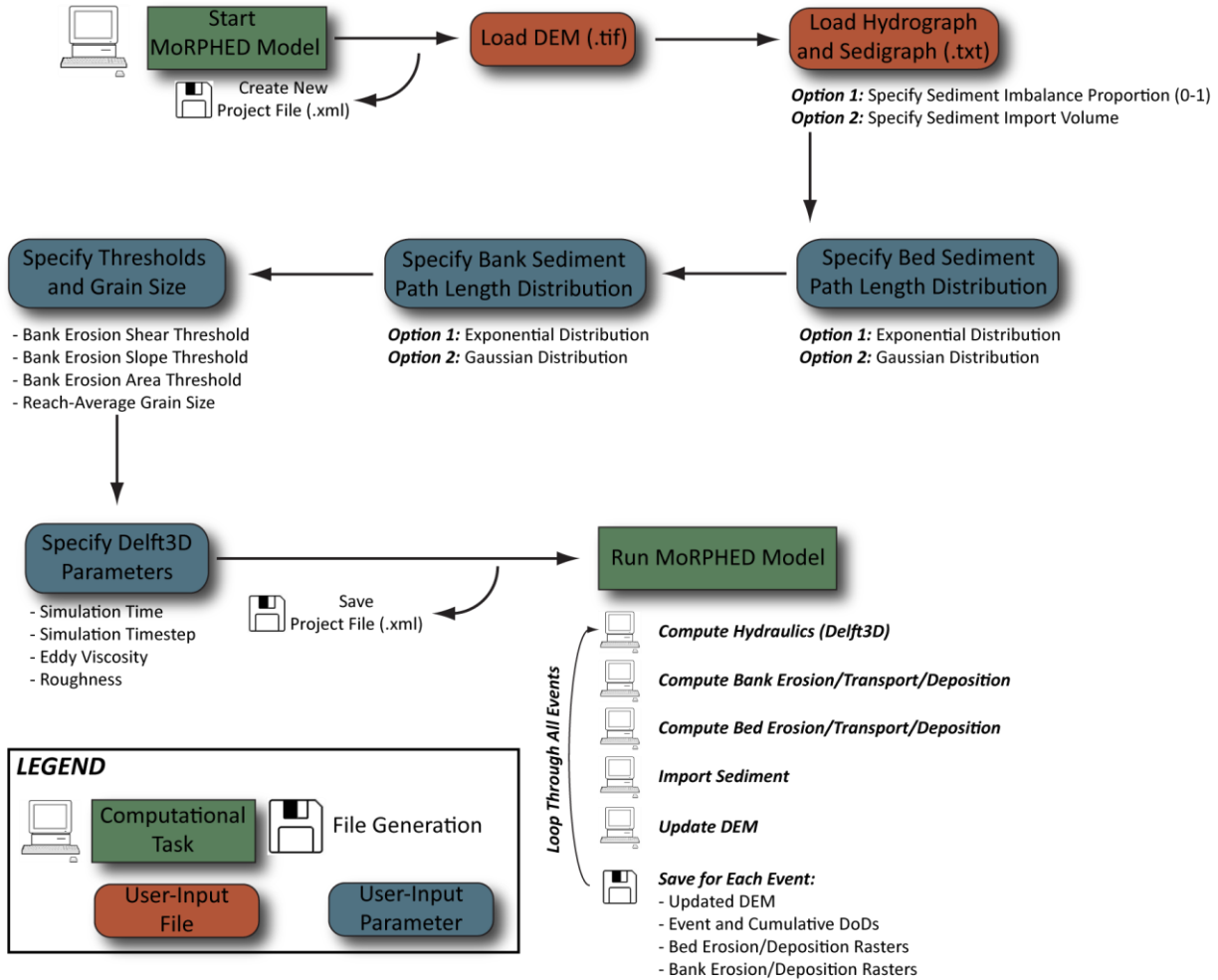


**TABLE 4.** River Feshie decadal modelling, geomorphic change detection results.

	<i>Field Raw</i>	<i>Field Thresholded (0.2 m)</i>	<i>MoRPHEd Raw</i>	<i>MoRPHEd Thresholded (0.2 m)</i>
<b>Areal</b>				
Total Area of Erosion (m <sup>2</sup> )	38,332	23,836	48,092	23,542
Total Area of Deposition (m <sup>2</sup> )	70,329	36,045	57,087	26,861
<b>Volumetric</b>				
Total Volume of Erosion (m <sup>3</sup> )	13,944	12,680	25,134	23,744
Total Volume of Deposition (m <sup>3</sup> )	18,264	14,677	15,712	13,748
<b>Vertical Averages</b>				
Average Depth of Erosion (m)	0.36	0.53	0.52	1.01
Average Depth of Deposition (m)	0.26	0.41	0.28	0.51
Average Total Thickness of Difference (m)	0.30	0.25	0.39	0.36
Average Net Thickness of Difference (m)	0.04	0.02	-0.09	-0.10



Figure 1.

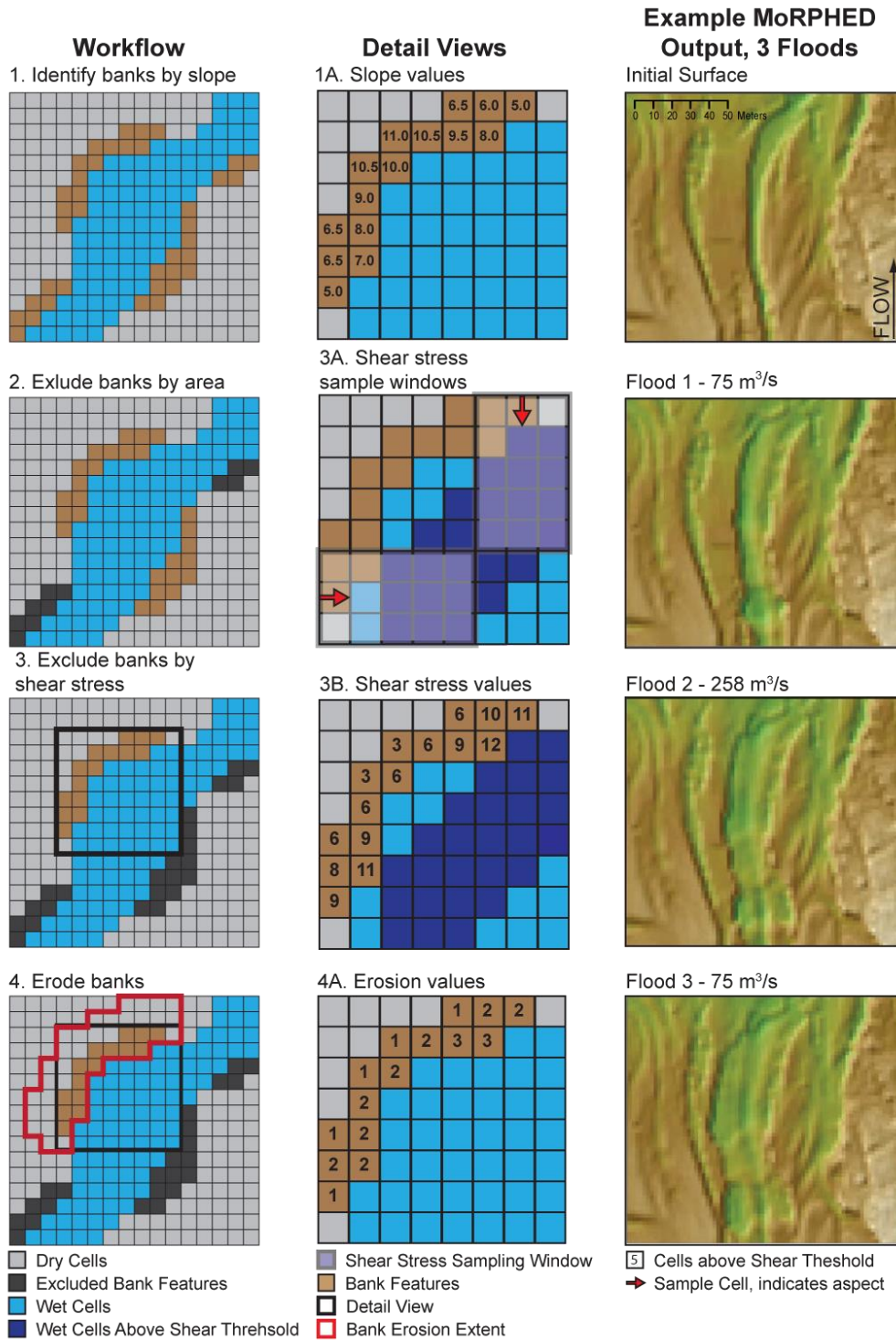


5

10

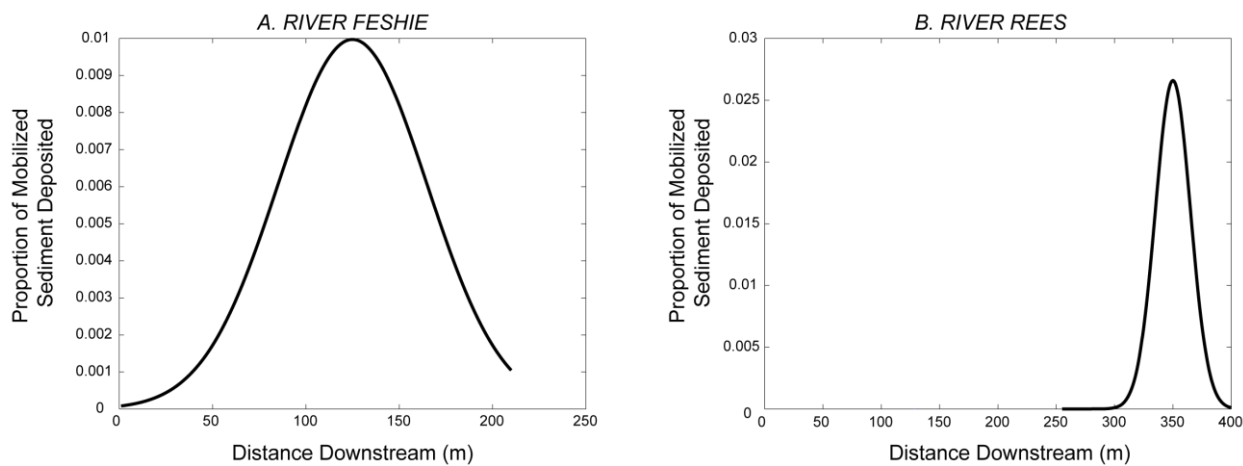


Figure 2.





**Figure 3.**



5

10

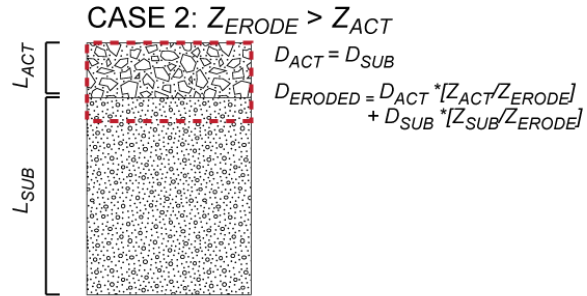
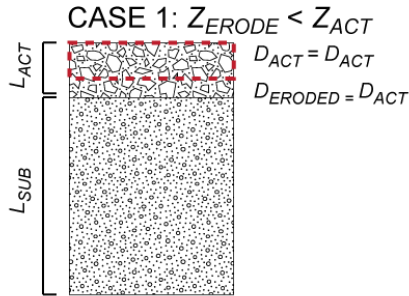
15

20

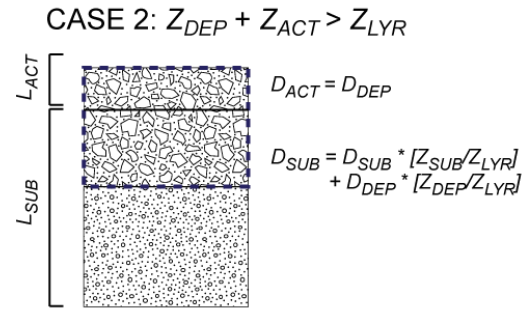
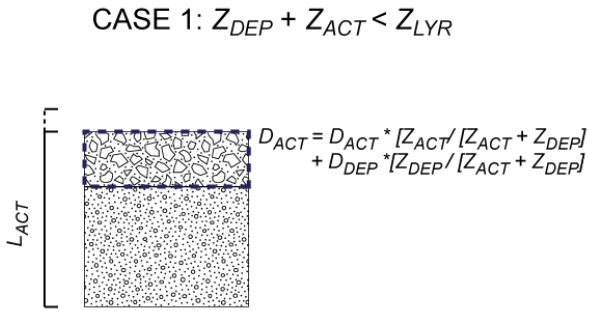


Figure 4.

**EROSION**



**DEPOSITION**



$Z_{ACT}$ : Thickness of Active Layer  
 $Z_{ERODE}$ : Thickness of Erosion  
 $Z_{DEP}$ : Thickness of Deposition  
 $Z_{LYR}$ : User-Defined Layer Thickness

$D_{ACT}$ : Grain Size of Active Layer  
 $D_{SUB}$ : Grain Size of Subsurface Layer  
 $D_{ERODE}$ : Grain Size of Eroded Sediment  
 $D_{DEP}$ : Grain Size of Deposited Sediment

5

10



**Figure 5.**

**River Rees, New Zealand**



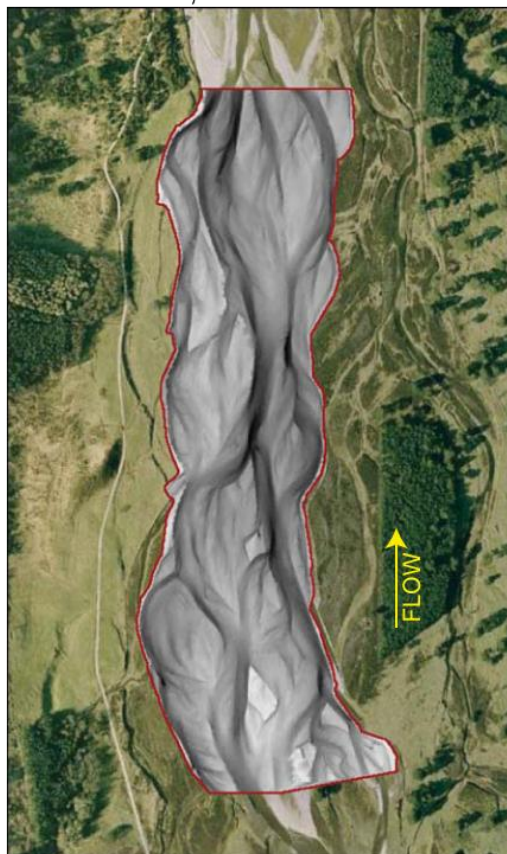
0 200 400 600 800 Meters

**Available Data: Rees**

**Event-Annual Scale:**

- Resurveys Following 10 Events over a 2-Year Timespan
- 15-Minute Hydrograph Record
- Existing Delft3D Hydraulic Modeling (Williams et al., 2013)

**River Feshie, Scotland**



0 50 100 150 200 Meters

**Available Data: Feshie**

**Annual-Centennial Scale:**

- Resurveys 2003-2007 & 2013
- 15-Minute Hydrograph Record
- Aerial Photographs since 1946
- Planform Maps Since 1869



Figure 6.

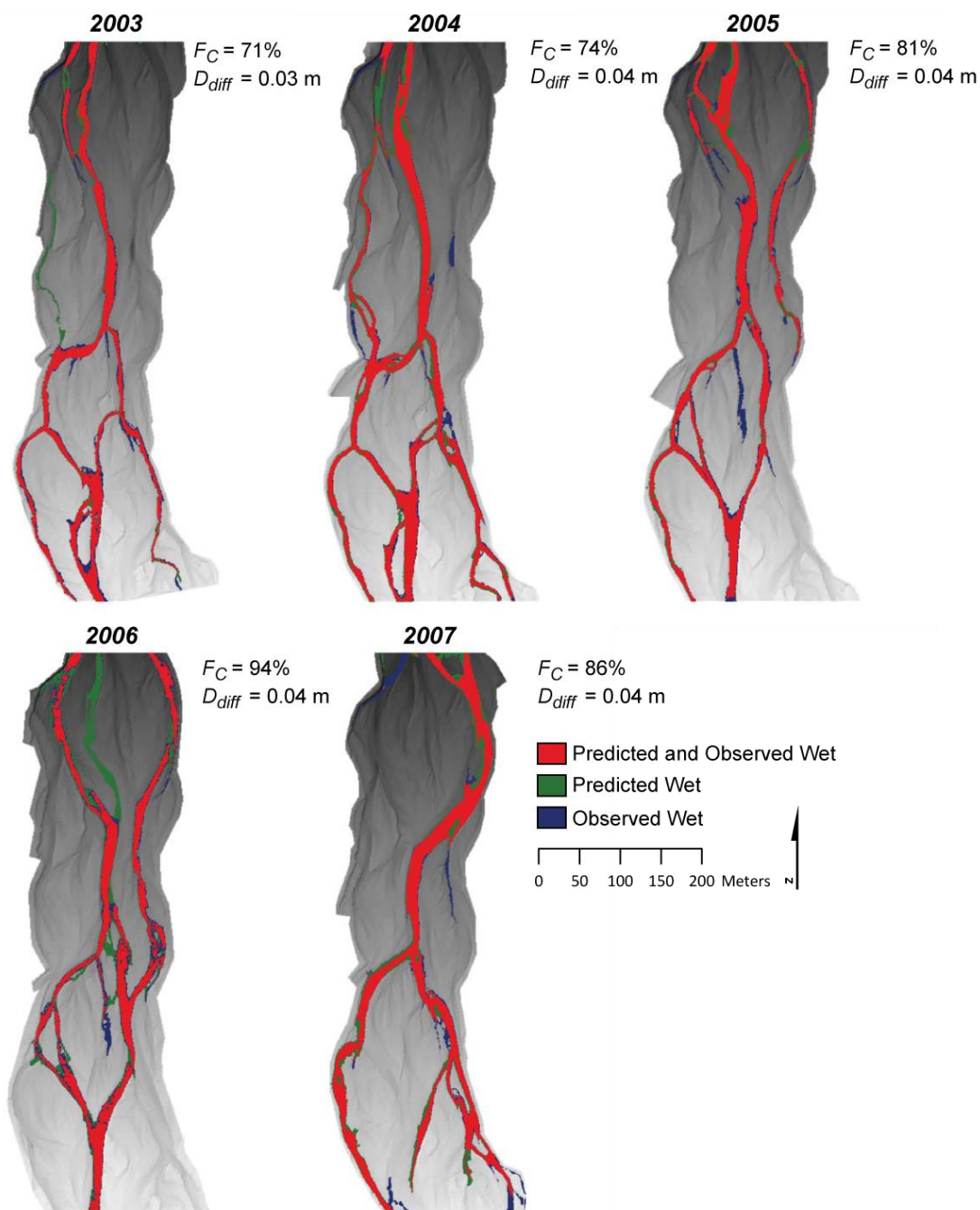




Figure 7.

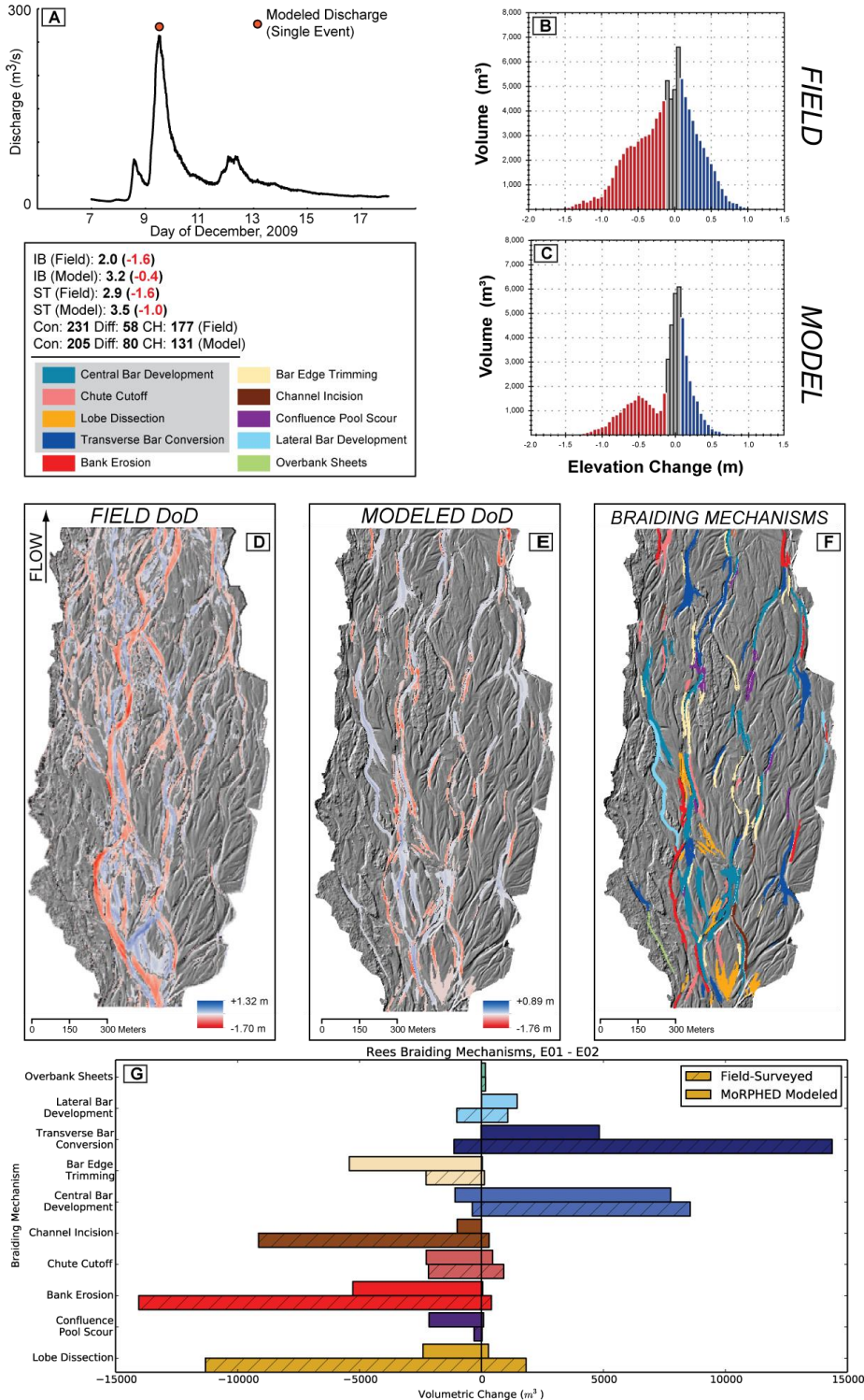
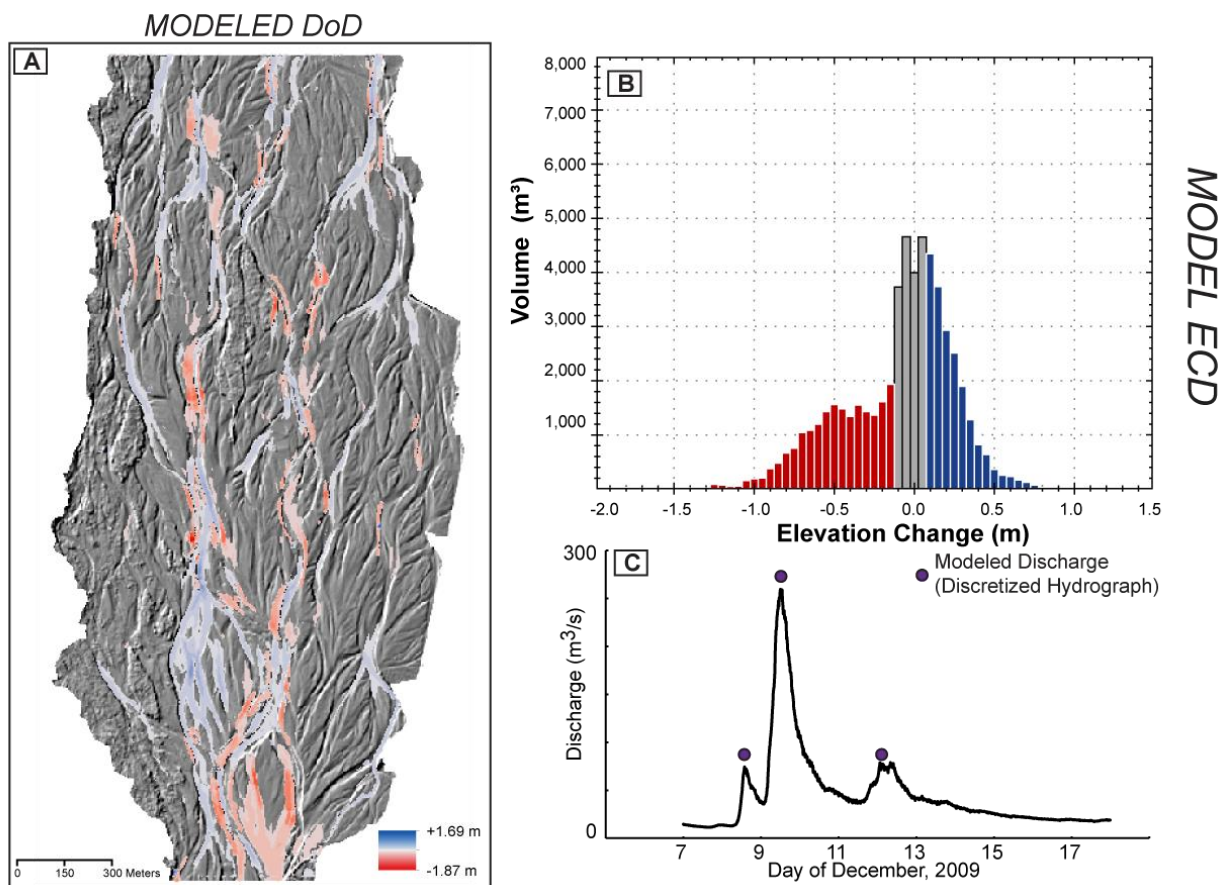




Figure 8.



5

10

15



Figure 9.

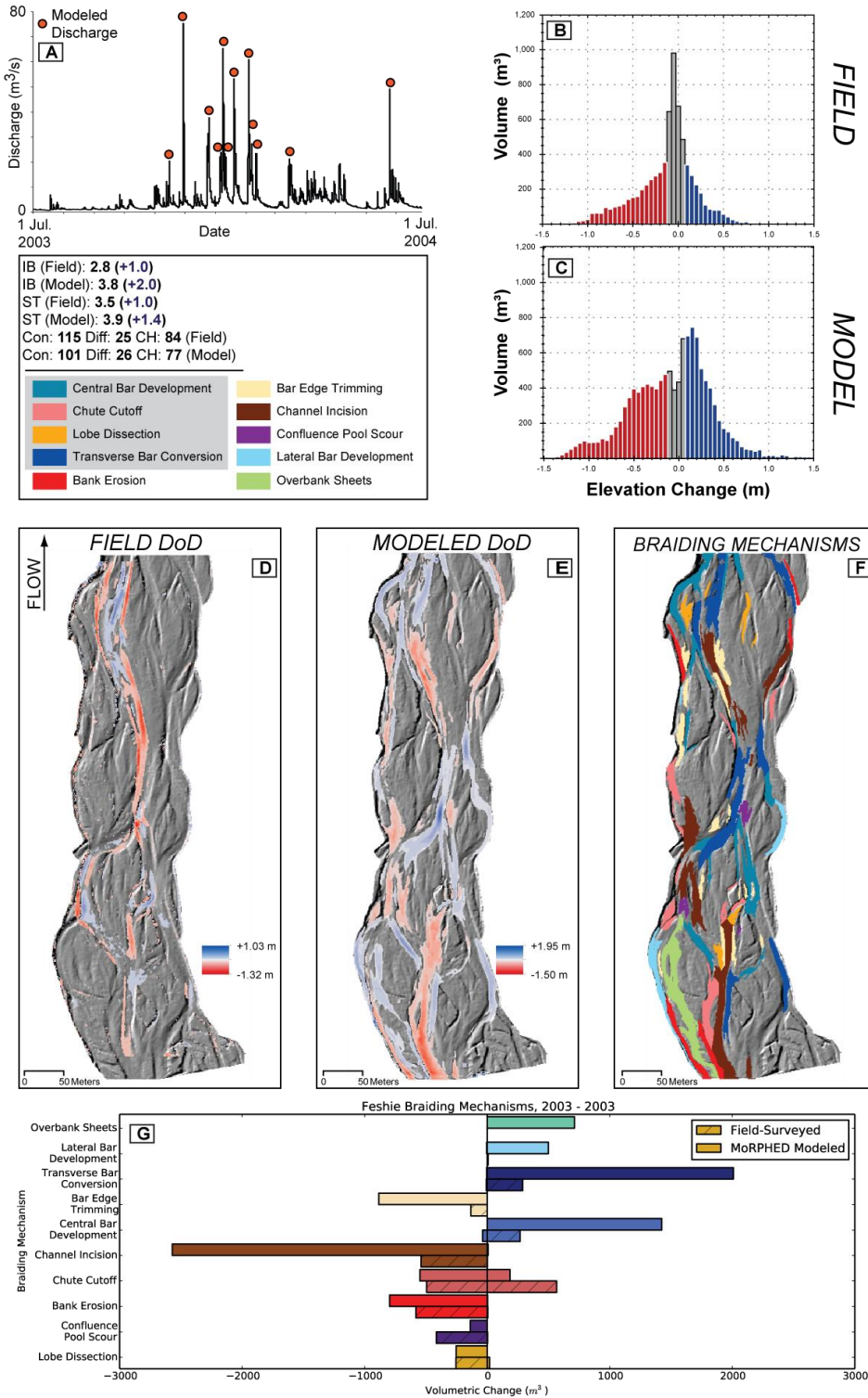
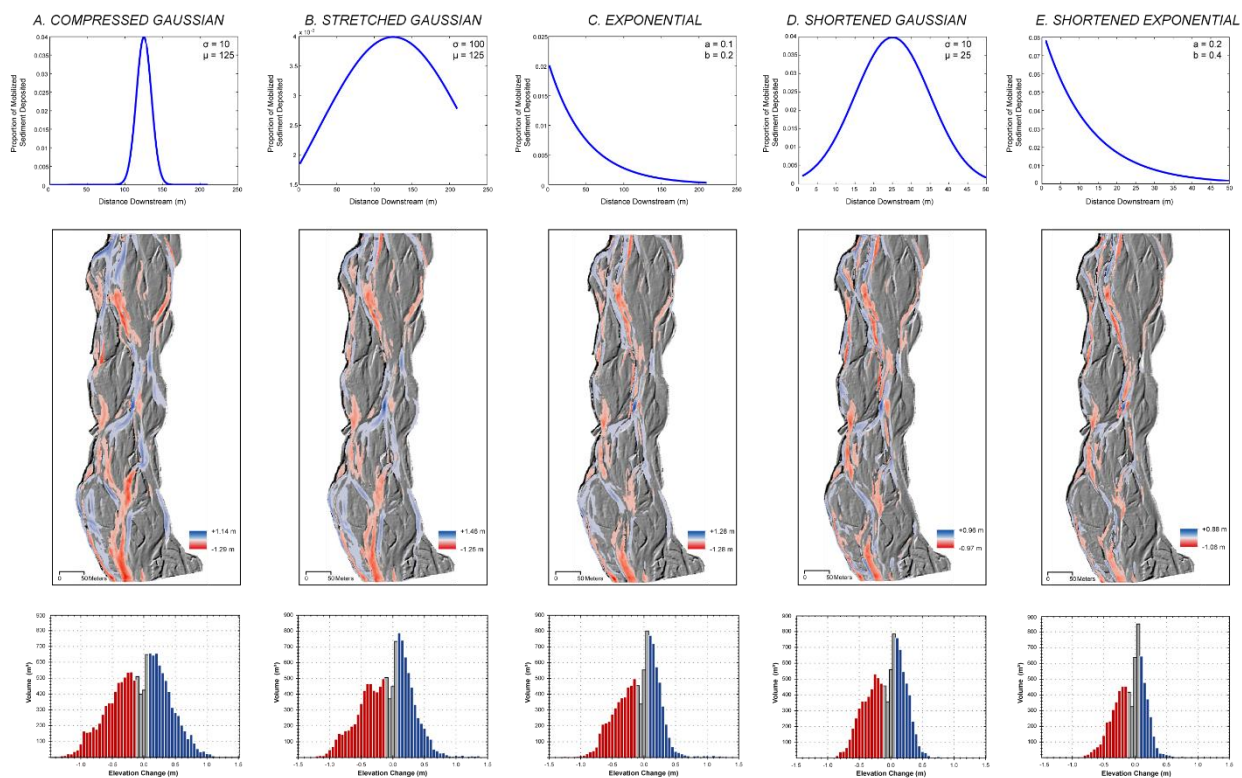




Figure 10.



5

10

15



Figure 11.

